European Research Infrastructure supporting Smart Grid Systems Technology Development, Validation and Roll Out

Technical Report TA User Project

PVGRIDHIL

Grant Agreement No:	**654113**
Funding Instrument:	**Research and Innovation Actions (RIA) – Integrating Activity (IA)**
Funded under:	**INFRAIA-1-2014/2015: Integrating and opening existing national and regional research infrastructures of European interest**
Starting date of project:	**01.11.2015**
Project Duration:	**54 month**

Contractual delivery date:	**28/11/2018**
Actual delivery date:	**23/11/2018**
Name of lead beneficiary for this deliverable:	**Alexis B. Rey Boué, UPCT**
Deliverable Type:	**Report (R)**
Security Class:	**Public (PU)**
Revision / Status:	**released**

Project co-funded by the European Commission within the H2020 Programme (2014-2020)

Document Information

Document Version: 1

Revision / Status: released

All Authors/Partners Alexis B. Rey Boué / UPCT
Johannes Stöckl / AIT

Distribution List **ERIGrid consortium members**

Document History

Revision	Content / Changes	Resp. Partner	Date
1	Full report	Alexis B. Rey Boué	23.11.18

Document Approval

Final Approval	Name	Resp. Partner	Date
Review Steering Com. Level	Thomas Strasser	AIT	

Disclaimer

Copyright Notice

Table of contents

Abbreviations

TA	Trans-national Access
UPCT	Universidad Politécnica de Cartagena
PV	Photovoltaic
CHIL	Controller-Hardware-in-the-Loop
RTDS	Real Time Digital Simulator
RCP	Rapid Control Prototyping
ADC	Analog-to-Digital converter
PWM	Pulse Width Modulation
LVRT	Low-Voltage-Ride-Through
VSI	Voltage Source Inverter
MPPT	Maximum Power Point Tracking
P	Instantaneous active power
Q	Instantaneous reactive power
PR	Proportional Resonant
DG	Distributed Generation
VHL	Very High Level
FPGA	Field-Programmable Gate Array
ASIC	Application-Specific Integrated Circuit
DER	Distributed Energy Resource
EU	European Union
PI	Proportional Integral
IGBT	Insulated Gate Bipolar Transistor
MOSFET	Metal-oxide-semiconductor Field-effect transistor
PNSD	Positive Negative Sequence Detector
V_{gf}	Depth of the grid voltage sag
S_{max}	Maximum apparent power when voltage sags occur
S_{nom}	Nominal apparent power (no voltage sags occur)
P_{max}	Maximum instantaneous active power during voltage sags
MPP	Maximum Power Point
DSOGI-FLL	Dual Second-Order Generalized Integrator Frequency-Locked Loop
MSOGI-FLL	Multiple Second-Order Generalized Integrators Frequency-Locked Loop

Executive Summary

The aim of this proposal is to implement vector control algorithms for grid-connected photovoltaic (PV) renewable systems in distorted and faulty utility grids. The algorithms will be tested by using the Controller-Hardware-in-the-Loop (CHIL) Simulation technique in which the power subsystem (including the PV Generator, the 3-phase inverter, the L filter and the utility grid) will be modelled using the software of PLECS RT Box 1, meanwhile the control subsystem will be modelled using SIMULINK blocks. The C-code will be generated using the Model-Based design approach and downloaded into a Real Time Digital Simulator (RTDS) for the former, and into a real microcontroller for the latter, running both in real time. The microcontroller will embed the control algorithms for its validation and the use of its peripherals will increase the reliability of the obtained results because the second order effects such as the quantization error of the ADCs, the computational and PWM delays, the dead time of the power switches of the inverter, the real utility grid with its output impedance, etc., will be considered, and what is more important, the same microcontroller (with the same hardware resources) could be used in a future real photovoltaic system with minor changes.

Firstly, the behaviour of the grid-connected PV system under harmonic distortions of the 3-phase utility grid voltages will be tested in order to find out its influence in the Power Quality of the inverter grid connection. Secondly, the effect of the unbalanced in the 3-phase utility grid voltages will also be investigated, mainly its effect on the second order harmonics in the dc bus voltage and in the detected fundamental frequency. Third, the effect of several sags in the 3-phase grid voltages will be investigated, as well as the Low-Voltage-Ride-Through (LVRT) capability of the control algorithms. Finally, the influence of the variation of the fundamental nominal frequency will also be studied.

1 General Information of the User Project

The main objective in this proposal is the implementation of the vector control algorithms to a PV grid-connected 3-phase Voltage Source Inverter (VSI). The VSI will be used as the power conditioner for the primary PV renewable energy source connected to the low-voltage 3-phase utility grid with disturbances. The block diagram of the proposal is depicted in the next Figure.

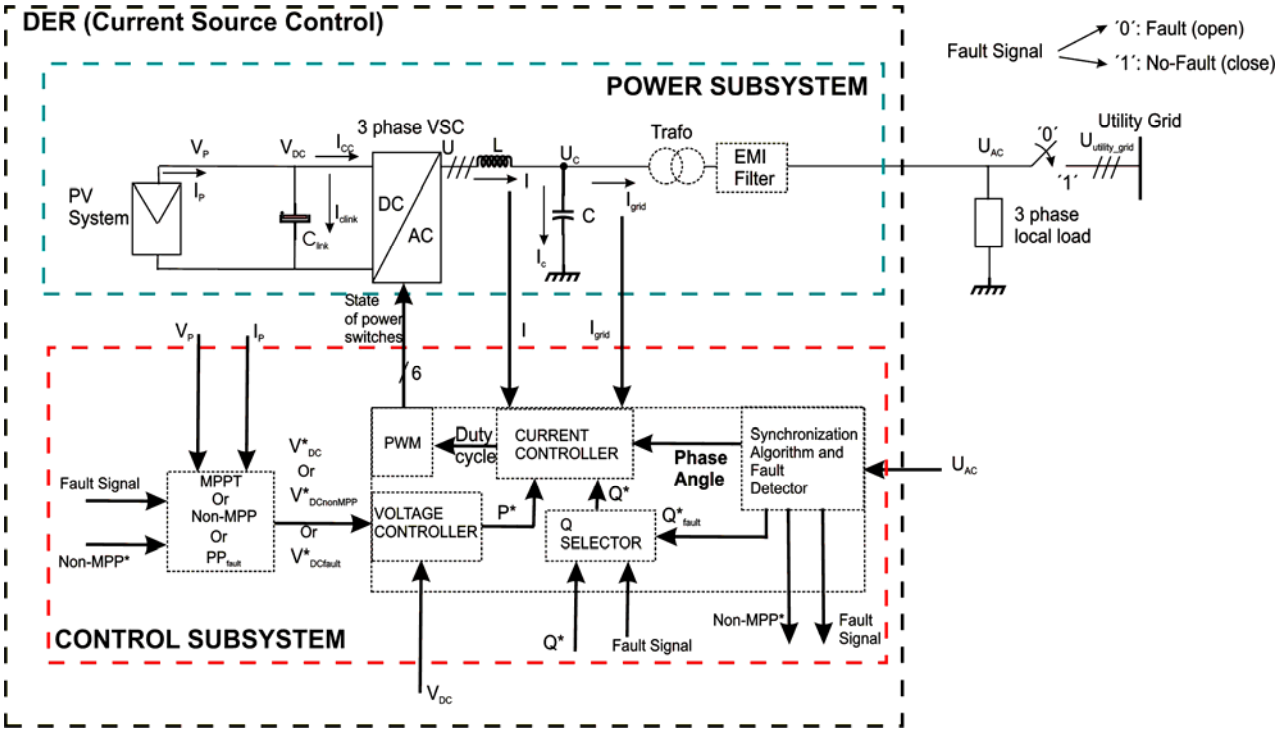

Figure 1: Block diagram of the Power and Control Subsystems for a 3-phase grid-connected system.

For grid-connected PV systems, the purpose is to control the power flow between PV modules and the utility grid with unity power factor and high power quality. The strong 3-phase utility grid behaves as sinusoidal voltage sources in series with highly inductive impedances and a current source vector control mode can be exerted. It is necessary that the PV system guarantees the maximum efficiency by controlling the power factor of the inverter-grid connection, making use of the reactive power theory which allows the control of the instantaneous active and reactive powers in decoupled d-q axes.

As can be seen in Figure 1, the Control Subsystem is fed by several sensed signals coming from the Power Subsystem and is the responsible of keeping the desired output even when perturbations occur at the input and output variables. Its main modules are the **Synchronization Algorithm and Fault Detector** for attaining a controllable power factor in the connection, the generation of a Fault Signal and the calculation of the non-MPPT when faults occur; the **MPPT (or non-MPP or PP_{fault})** algorithm in order to compute the needed DC bus voltage command (V^*_{DC}) for extracting the maximum available power of the PV generator for a specific irradiance and temperature (or the non maximum power when fault occurs); the innermost **CURRENT CONTROLLER** loop, and the outermost **VOLTAGE CONTROLLER** loop.

The outermost loop regulator compares the DC voltage in the Link capacitor (V_{DC}) with the reference which comes from the block that executes the MPPT and non-MMPT algorithm and the error feeds a PI regulator. The output of this regulator is the active power reference command (P^*), meanwhile the **Q SELECTOR** block selects the reactive power reference command (Q^*) for fault and no-fault operation. Both P* and Q* are responsible of the generation of the α-β current reference commands for the innermost control loop. This loop not only uses two Proportional Resonant (PR) controllers in

αβ axes to regulate the α-β components of the 3-phase line currents, but also several resonant controllers to compensate the low order harmonic perturbation of the utility grid voltages. The output of the current regulator feeds the **PWM** block in order to generate the switching signals for the 3-phase VSI.

It must be pointed out that when a short duration fault occur, the updated international Grid Codes impose to the PV system not to disconnect from the utility grid, but instead it must inject a certain amount of reactive power and, in some cases, active power, together with a limitation in the amplitude of the line currents sets to its nominal value. This is known as Low-Voltage-Ride-Through (LVRT) capability and will be implemented as well.

In this work, the objective will be fulfilled with the use of the **Controller-Hardware-in-the-Loop (CHIL) Simulation technique**: the PV modules, the 3-phase inverter, the L filter and the 3-phase low-voltage utility grid will be modelled and run in real time, whereas a real microcontroller will embed the control algorithms for its validation. Although an experimental platform can be built for an only one renewable source, the approach of this Project avoids the increase of the overall cost when several renewable sources are scaled in order to build a Distributed Generation (DG) system. Then, after the validation of the tests carried out in the CHIL setup for one PV renewable source, other renewable sources such as critical loads, storage elements, wind turbines, etc. can be easily added in order to test the interaction between them, the perturbation on the voltage and frequency profile of the public utility grid, but at the same time the safety of the whole system and operators will be guaranteed.

The TA infrastructure must have **two hardware units** and instrumentation tools with recording facilities. One of the units will be used as the Real Time Digital Simulator (RTDS) for the Power subsystem, meanwhile the second unit will be used as the controller board for the Control subsystem. Both units could be programmed using MATLAB/SIMULINK [1] or another Very High Level (VHL) simulation tool (called Model-based Design) and run in real time, meanwhile several measurements to the output signals of the corresponding voltage, current and power of the model, among others, will be firstly displayed in an oscilloscope for monitoring purposes, and secondly recorded for further evaluation. OPAL-RT and Typhoon HIL are the world leader companies in the development of real time digital simulation and HIL electronic systems.

Number of tests to be carried out (see Figure 2):

1. A **real-time digital simulation** of a grid-connected PV system with a distorted and unbalanced 3-phase low-voltage utility grid will be carried out in order to get familiar with the VHL simulation tool and one of the hardware units employed. In this case, some measurements with the oscilloscope will validate the test.
2. The **CHIL technique** is implemented, using two hardware units and test 1 is repeated for a distorted utility grid. In this case, the use of a real controller (i.e. OPAL-RT) working as a Rapid Control Prototyping (RCP) scheme and its peripherals will increase the reliability of the obtained results because all the second order effects such as the quantization error of the ADCs, the computational and PWM delays, the dead time of the power switches of the inverter, the real networks with its output impedance, etc. will be considered. The influence of the control algorithm in the mitigation of the harmonic contamination of the 3-phase utility grid currents and so, the increase of the Power Quality of the inverter-grid connection, will be investigated.
3. The same as test 2, but for unbalanced 3-phase low-voltages. The influence of the control algorithm on the second order harmonics in the DC bus voltage and in the detected fundamental frequency will be investigated.
4. The same as test 2, but several voltage sags are imposed to the utility grid and the LVRT capability will be tested.

5. The same as test 2 when the fundamental nominal frequency varies. In this case, the reliability of the control algorithm will be tested.

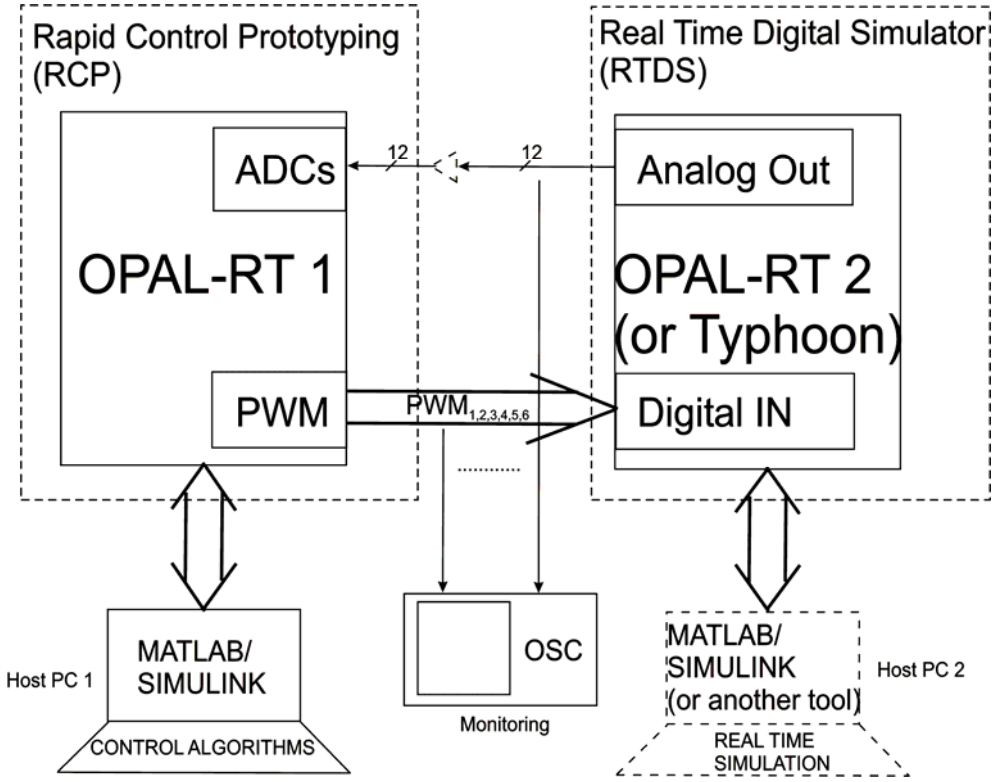

*Figure 2: Block diagram of the **proposed** CHIL Simulation test setup.*

Considering that if the RTDS and the RCP are of the same company, no restrictions should be attained regarding the electrical characteristics for interfacing the output/input signals, and a plug & play behaviour could be expected. On the contrary, for different manufacturers (i.e. OPAL-RT, Typhoon, etc.), special care must be observed in the connection of both electronic units, and eventually an electronic interface circuit would be designed.

It is worth noting the absence of power interchange in the proposal, making the test setup a safe environment not only for the electronic boards, but also for actual and future users without losing the physical meaning of the attained results if very accurate models of the power subsystem are used. The robustness and realistic of the proposal is ensured by the fact of several papers published by the authors in the same field of research, mainly with a RTDS setup, but extensible to CHIL Simulation. Regarding the latter, several tests have been done by the authors as a result of a 36 months-duration National Research Project in Spain, although an average model for the 3-phase inverter was used due to a limitation in the hardware resources of the RTDS board employed.

Finally, we think that the time consuming for getting familiar with OPAL-RT, Typhoon, or any other tool and their VHL Simulation tool environment is certainly unknown, as well as for the debugging of the control algorithms, making the fulfilment of the project objectives a little risky. However, the authors have experienced in the Model-based Design technique with similar environments (DSPACE and SIMULINK) and with the development of several enhanced control algorithms for grid-connected inverters, which makes this uncertainty affordable.

It is intended to develop and test new algorithms for vector control of Voltage Source Inverters (VSI) used in the control of a PV renewable system connected to the perturbed low-voltage 3-phase utility grid. The Model-based design will be used to develop the control algorithms starting from models in SIMULINK (or another dynamic simulation tool), generating C-code automatically and download

them into the controller; the same idea can be applied to the models of the power subsystem that will be run in the Real Time Digital Simulator. Although it is not possible to debug the control algorithms in a real situation due to the public nature of the utility grid, they will be debugged and tested in a distorted, unbalanced and faulty utility grid with the use of the CHIL Simulation technique, yielding an innovative and cheap approach to impose several tests in order to explore its behaviour to the several perturbations and faults in the utility grid voltages, but at the same time avoiding the power interchange in the test setup which contributes to a safer environment for the electronic circuits and users, avoiding possible failures during the debugging process.

On the other hand, once the control algorithms are validated in the test setup, the authors believe that the same algorithms could be implemented in a real microcontroller, in an FPGA device, or even in an ASIC (customizing the design) in order to test them in a real power installation with minor changes, for its final validation. Moreover, several PV systems (with different nominal rated power) can be scaled in order to arrange several Distributed Energy Resources (DER) for a Distributed Generation (DG) scenario, although a fast communication system must be implemented if a MASTER-SLAVE configuration is set. The latter will facilitate definitely the integration of renewable energy systems into the European electrical system.

The impact of the results of this work will contribute to the increased use of more and more renewable energy sources in the EU, to reduce the fossil fuels dependency, and to promote a low carbon economy, as well as to the sustainable growth in the economy. In addition, it will contribute to decrease the total emissions of polluting gases in order to reduce its negative impact on the environment and then, agree to European legislations, making possible the sustainable growth in a near future. Moreover, some standards and technical specifications (i.e. harmonics fault regulations) for products, process, etc. could be attained in order to ensure interoperability and safety between European companies, and what is more important, these aspects could improve the competitiveness of European industries in a globalized world.

European people will understand firstly some negative impacts of human activities on the environment, and secondly that the ways towards its long-term mitigation will deal with the Research and Innovation activities. It will be mandatory the implementation of roadmaps indicating the steps to be followed in order to make our planet a safer place to live, with a green economy, and less risks to human health. In addition, the assumption of a less risky green economy implies that new jobs might necessarily be created so as to be able to deal with new scientific and technologic paradigms, which would also contribute to the decrement of the unemployment.

The results of the research and innovation activities will be available for all the European citizens, no matter what countries they are from, what religion they profess or what race they have. So, in the global values of freedom and democracy, the equality among them will be reinforced, and a safer place to live healthy will be a fact. This aspects will contribute to the integration and cohesion among all the European people.

The European energy union will contribute to a climate-friendly energy and to a low-carbon, secure and competitive economy. Energy will flow freely across national borders.

In short, we think that the proposed work will facilitate definitely the integration of PV renewable energy systems into the European electrical system.

The following research projects are involved in the design of the control algorithms for grid-connected converters. So there are a high synergy with the actual ERIGrid proposal in the approach, scope and objectives.

1. Title: OPTIMIZACION DEL DISEÑO Y CONTROL DE CONVERTIDORES AC/DC PARA LAS NUEVAS PLANTAS SOLARES DE 1500V CON CONEXION A LA RED ELECTRICA (Optimization of the design and control of AC/DC converters for new 1500V grid-connected Solar Plants)
   Funded: Ministerio de Economía, Industria y Competitividad, Spain (http://www.mineco.gob.es/)
   Reference: DPI2017-88505-C2-2-R
   Entity: Escuela Técnica Superior, Universidad de Alcalá, Spain
   Main Researcher: Santiago Cóbreces Álvarez

2. Title: CONTROL Y GESTIÓN DE NANORREDES AISLABLES: ESTRATEGIAS DE CONTROL PARA NANORREDES AISLABLES (Control and management of nanogrids with standalone mode capability: Control Strategies for nanogrids with standalone mode capability)
   Funded: Ministerio de Economía, Industria y Competitividad, Spain (http://www.mineco.gob.es/)
   Reference: TEC2016-77632-C3-1-R
   Entities: Universidad de Cádiz; Universidad de Córdoba; Universidad de Extremadura, Spain
   Main Researcher: Eva González Romera

2 Research Motivation

The setup scheme used in this project embed the control algorithms in a real microcontroller for its validation. So, the use of its peripherals will increase the reliability of the obtained results because all the second order effects such as the quantization error of the ADCs, the computational and PWM delays, the dead time of the power switches of the inverter, the real utility grid with its output impedance, etc., will be considered, and what is more important, the same real controller (with the same hardware resources) could be used in a future real PV system with minor changes.

Although the experimental platform was built for an only one renewable source, the approach of this Project can be extrapolated when several renewable sources are scaled in order to build a Distributed Generation (DG) system. So, after the validation of the tests carried out in the CHIL setup for one PV renewable source, other renewable sources such as critical loads, storage elements, wind turbines, etc. can be easily added in order to test the interaction between them, the perturbation on the voltage and frequency profile of the public utility grid, but at the same time the safety of the whole system and operators might be guaranteed.

Finally, it is worth noting that a more powerful RTDS with more hardware resources and smaller sample times, i.e. using FPGA devices, must be employed if the testing of a DG system is needed.

2.1 Objectives

The main objective in this proposal was the implementation of the vector control algorithms to a PV grid-connected 3-phase Voltage Source Inverter (VSI). The VSI will be used as the power conditioner for the primary PV renewable energy source connected to the low voltage 3-phase utility grid with disturbances. See Figure 1.

3 State-of-the-Art

The aim of the high penetration of PV Systems into the utility grid nowadays is the mitigation of the

greenhouse effect and environment pollution, together with the reduction of fossil fuel, coal and nuclear energy dependency, which has led to new paradigms in the control approach for the power converter. In general, the incoming power injected into the grid by the grid-connected PV systems will perturb the voltage and frequency profile of the public utility grid, decreasing the power quality and making the grid stability a challenging task unless an enhanced control strategy were used.

In most cases, the power converter will be a Voltage Source Inverter (VSI) that will transform the DC nature of the input power to the AC nature of the output one, according to its design and load specifications. For grid-connected PV systems, the purpose is to control the power flow between the PV Generator and the utility grid, as well as the power factor of the inverter-grid connection with high power quality; the power flow is achieved with a voltage controller allowing the proper DC bus voltage in a link capacitor according to the maximum power point of the PV panels in **normal operation mode** [2], meanwhile the power factor is controlled with a current controller that must also compensate the harmonic contamination of the utility grid voltages [2-4]. Moreover when short-duration faults occur in the grid voltages, the inverter must not be disconnected from the grid and, according to the Grid Code, an ancillary service known as Low-Voltage-Ride-Through (LVRT) capability [5,6] must be ensured to inject a certain amount of reactive power to improve the voltage profile during the fault, but not exceeding the nominal value of the 3-phase currents in order to protect the inverter from overcurrent failure.

Several strategies can be employed for the vector control of the 3-phase line currents of the inverter. Among them, d-q control with PI regulators, hysteresis control, deadbeat control and, more recently, proportional-resonant (PR) controllers in α-β axes are the most widely used [3]. The current vector control must guarantee the highest power quality, together with a controllable power factor of the inverter-grid connection.

When the d-q control strategy is used, it will appear the second harmonics 2ω in the instantaneous active (P) and reactive (Q) powers when unbalanced faults occur because the negative- sequence of the 3-phase utility grid voltages are not used in the calculation of the current references i^*_{dq}, although the 3-phase line currents will be completed balanced and limited in its amplitude to deal with the Grid Code requirements (see Figure 3). On the contrary, if the PR controllers in α-β axes are applied, a Current References Generator could cancel the second order harmonics of P and/or Q because in this case the negative- sequence of the 3-phase utility grid voltages are used to compute the current references $i^*_{\alpha\beta}$ (see Figure 4), although the 3-phase line currents might be unbalanced or balanced sinusoidal or distorted according to the strategy used [6,7]. In both cases the output of the current regulator feeds the PWM block through the inverse Park (dq→abc) and Clarke (αβ→abc) transformations, respectively, in order to generate the switching signals for the power-switches of the 3-phase VSI.

As said before, in **normal operation** the maximum available power in the PV modules must be injected into the utility grid. For this, an algorithm capable of obtaining the maximum power at a given irradiance and temperature is needed, known as Maximum Power Point Tracking (MPPT) algorithm. On the contrary, in **fault operation mode**, the LVRT capability is activated to improve the grid voltage profile during the fault.

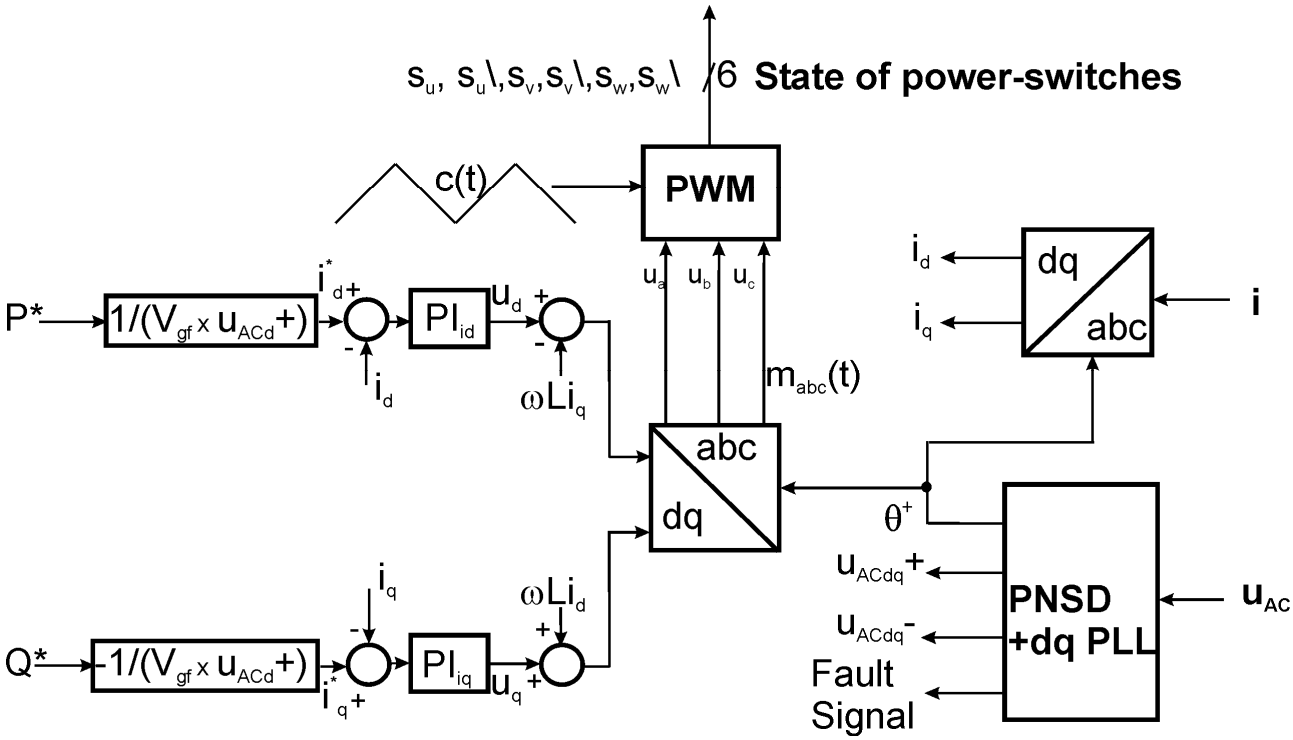

Figure 3: Block diagram of a grid-connected PV Generator using the dq control strategy with PI regulators for the 3-phase line currents and with LVRT capability.

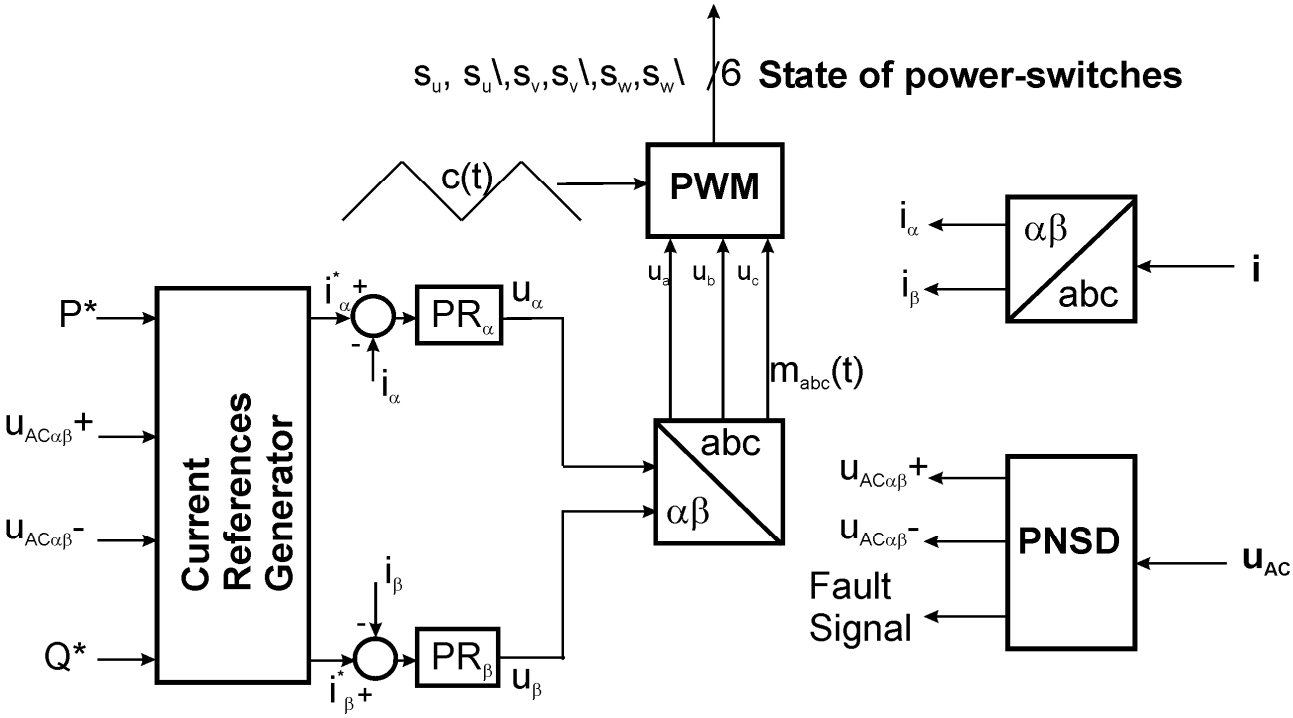

Figure 4: Block diagram of a grid-connected PV Generator using the PR controller for the 3-phase line currents and with LVRT capability.

According to the previous Figure, the outputs of the **Current References Generator** block are:

$$i_{\alpha}^{*} = \frac{v_{AC\alpha}^{+} - v_{AC\alpha}^{-}}{(v_{AC\alpha}^{+\,2} + v_{AC\beta}^{+\,2}) - (v_{AC\alpha}^{-\,2} + v_{AC\beta}^{-\,2})} P^{*} + \\ + \frac{v_{AC\beta}^{+} + v_{AC\beta}^{-}}{(v_{AC\alpha}^{+\,2} + v_{AC\beta}^{+\,2}) - (v_{AC\alpha}^{-\,2} + v_{AC\beta}^{-\,2})} Q^{*} \quad (1)$$

$$i_{\beta}^{*} = \frac{v_{AC\beta}^{+} - v_{AC\beta}^{-}}{(v_{AC\alpha}^{+\,2} + v_{AC\beta}^{+\,2}) - (v_{AC\alpha}^{-\,2} + v_{AC\beta}^{-\,2})} P^{*} - \\ - \frac{v_{AC\alpha}^{+} + v_{AC\alpha}^{-}}{(v_{AC\alpha}^{+\,2} + v_{AC\beta}^{+\,2}) - (v_{AC\alpha}^{-\,2} + v_{AC\beta}^{-\,2})} Q^{*}$$

and the oscillating component of the instantaneous active power (P) at 2ω (ω is fundamental nominal frequency) is drastically reduced [6].

On one hand, the utility grid voltage has several disturbances such as harmonic distortions, unbalances, as well as faults. Moreover, the inverter used in the grid-connected renewable sources produces high frequency ripples due to the switching nature of the electronic device (IGBT or MOSFET), which adds some negative effects in the power quality. On the other hand, the connection of renewable sources to the utility grid must be properly controlled according to the expected operating conditions of the primary energy source (different values of irradiance and temperature for Photovoltaics, variation of wind speed for Wind Power Systems, quantity of energy in the Fuel Cell, etc.) and to the utility grid conditions (Unity Power Factor operation, synchronization, islanding protections, etc.). So, simulation tools have been commonly used in the last years to validate the control algorithms and deal with this situation, although less fidelity will be achieved because the modelling of the second order effects such as the quantization error of the ADCs, the computational and PWM delays, the dead time of the power switches of the inverter, the real networks with its output impedance, etc., are not always affordable.

For both modes of operation, experimental results can be successfully achieved in real platforms for one renewable primary source, where new vector control algorithms have been designed focusing on improving the performance of the connection of the primary renewable energy source to the low-voltage 3-phase utility grid. However, the debugging and validation of these algorithms are difficult to be carried out in a real scenario with distributed generation (DG) where a high penetration of several renewable source systems is a fact, due to the increase of the overall cost of the installation together with the impediment of exerting control tests to evaluate its behaviour, the interaction of them and its influence on the voltage and frequency profile of the public utility grid.

To overcome these drawbacks, the **(Power) Controller-Hardware-in-the-Loop Simulation** technique is a novel approach nowadays. The power subsystem (including the 3-phase inverter) is modelled in a **Real Time Digital Simulator (RTDS)**, whereas the control algorithms are embedded in a **real controller** that will be fed by the output signals coming from the RTDS (sometimes an electronic interface is needed), both run in real time for the behaviour validation [8,9]. The use of a real controller and its peripherals will increase the reliability of the obtained results because all the second order effects mentioned above will be considered, and what is more important, the same real controller might be used in a future real power system with minimal changes.

Several platforms can be used to build the setup for CHIL, among them, dSPACE [10], OPAL-RT Technologies [11], Typhoon HIL [12], etc. Several scenarios arise according to the complexity of the plant to be modelled, its hardware resources, the minimum available sample time, its cost, etc. So,

the user must study in detail these features in order to make the best choice to build the test setup.

4 Executed Tests and Experiments

4.1 Test Plan

Table 1: Proposed tasks of the Project.

Week	*Task*	*Time*
1	A **real-time digital simulation** of a grid-connected PV system with a distorted and unbalanced 3-phase low-voltage utility grid will be carried out (one hardware unit working as an RTDS and an oscilloscope are needed).	1.10.2018-5.10.2018
2	The **HIL technique** is implemented, using two hardware units (one hardware unit working as the controller board; a second hardware unit working as the RTDS) and task 1 is repeated for a distorted and an un-balanced utility grid.	8.10.2018-12.10.2018
3	The same as task 2, but several voltage sags are imposed to the utility grid and the **LVRT** capability will be tested.	15.10.2018-19.10.2018
4	The same as task 2 when the fundamental nominal frequency varies. In this case, the reliability of the control algorithm will be tested.	22.10.2018-25.10.2018

All the tests were run using the block diagram of the setup depicted in Figure 6, with PLECS RT Box 1 [13] for the Power Subsystem and the TMS320F28379D microcontroller [14] for the Control Subsystem. A photo of the setup is depicted in Figure 5.

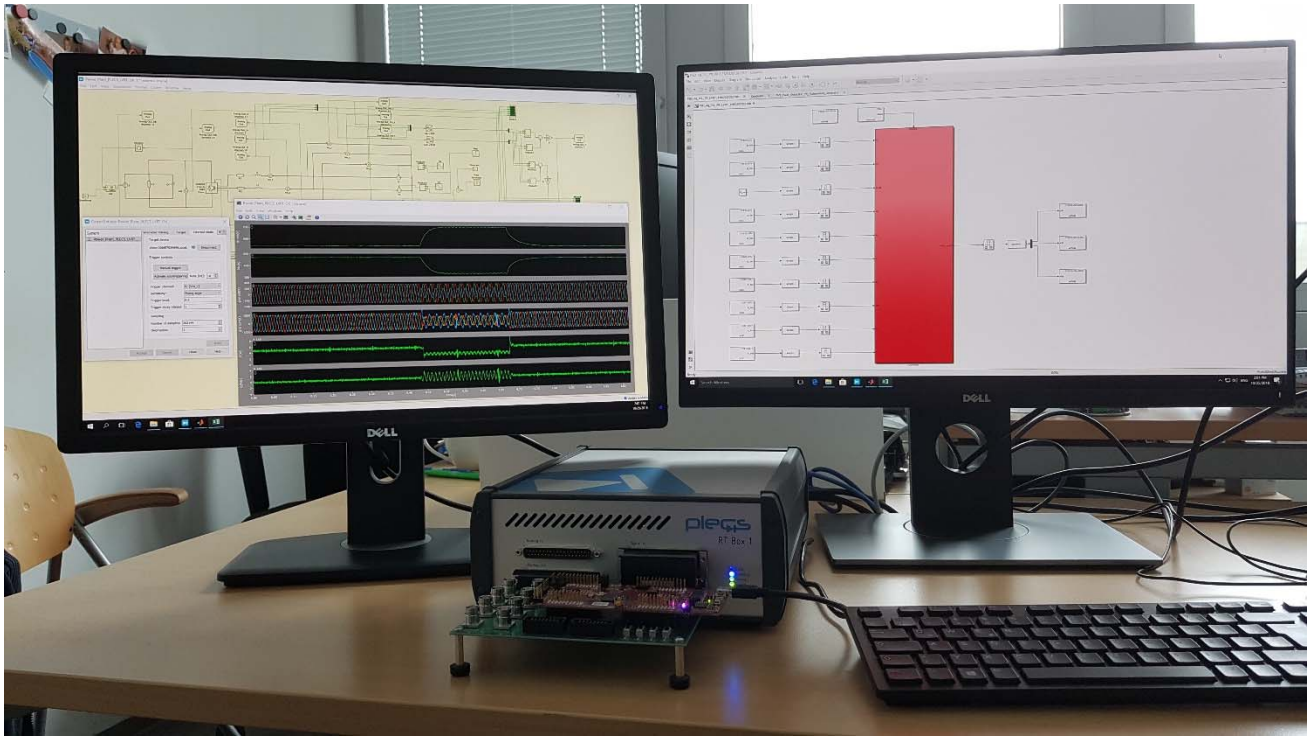

Figure 5: Photo of the setup for the tests carried out using the CHIL Simulation Technique.

The following Tables show the parameters of the Power and Control Subsystems:

Table 2: Parameters of the 320W PV module Suntech STP320-24-Ve polycrystalline.

Parameters	***Value***
Maximum power	P_{mp} = 320,024W
Maximum power voltage	V_{mp} = 36,7V
Maximum power current	I_{mp} = 8,72A
Open circuit voltage	V_{oc} = 45,6V
Short circuit current	I_{sc} = 9,07A
Cell number per module	N_{cell} = 72
Temperature coefficient of I_{sc}	α_i = 0,0867/°C
Temperature coefficient of V_{oc}	α_v = -0,4278/°C
Parallel resistance	R_p = 4.240,74Ω
Series resistance	R_s = 0,3437Ω
Ideally factor of the diode	m = 1,1238

Table 3: Parameters of the proposed PV array (PV Generator).

Parameters	***Value***
Number of the strings	N_{pvst} = 72
Number of the series modules	N_{pvs} = 22
Maximum current	$I_{mpv} = N_{pvst} \times I_{mp}$ = 627,84A
Maximum voltage	$V_{mpv} = N_{pvs} \times V_{mp}$ = 807,4V
DC output power	$P_{dc} = V_{mpv} \times I_{mpv}$ = 506,91kW
Open circuit voltage	$V_{PV\text{-}oc} = N_{pvs} \times V_{oc}$ = 1.003,2V
Short circuit current	$I_{PV\text{-}sc} = N_{pvst} \times I_{sc}$ = 653,04A

The PV Generator is modelled using a Lookup Table (2-D) for different irradiance values G as shown in Table 4:

Table 4: Lookup table for the PV Generator built with the 320W PV module Suntech STP320-24-Ve polycrystalline

	G_1=0,2kW/m^2	G_2=0,4kW/m^2	G_3=0,6kW/m^2	G_4=0,8kW/m^2	G_5=1kW/m^2
V	I	I	I	I	I
0,633809785	132,5368722	265,0694088	397,5976098	530,1214752	662,641005
30,73224907	132,5322267	265,060118	397,5836736	530,1028937	662,617778
60,83068843	132,527581	265,0508269	397,5697371	530,0843116	662,59455
90,92912796	132,5229348	265,0415352	397,5557997	530,0657284	662,571321
121,0275678	132,5182878	265,0322423	397,5418607	530,047143	662,548089
181,2244498	132,5089872	265,0136476	397,5139706	530,0099557	662,501602
209,3163306	132,5046399	265,0049605	397,5009422	529,9925839	662,479884
241,4213418	132,4996589	264,9950152	397,4860293	529,9726987	662,45502
271,5197983	132,4949655	264,9856592	397,4720045	529,9539967	662,431629
309,6445346	132,4889514	264,9737144	397,4541122	529,930134	662,401765
329,7102062	132,4857279	264,9673485	397,4445875	529,9174283	662,385848
359,8087646	132,4807504	264,9576064	397,4300379	529,8980127	662,361487
389,9074339	132,4754636	264,9474438	397,4149165	529,8778199	662,33607
420,0063175	132,4695795	264,9364691	397,3986911	529,8561261	662,308612
450,1056149	132,4625419	264,9239262	397,3803338	529,8315341	662,277214
480,2057114	132,4532767	264,9083551	397,3578596	529,8013453	662,238207
510,307351	132,43971	264,886936	397,3274353	529,7603484	662,184507
540,4119704	132,4178367	264,8542243	397,2816589	529,6984805	662,102433
570,522344	132,3799227	264,7997055	397,206236	529,5963089	661,965566
600,6438295	132,3110326	264,7030754	397,0735636	529,4163075	661,722892
630,786773	132,1823255	264,525125	396,8303377	529,0860106	661,275894
660,9711537	131,9381067	264,1901385	396,3736241	528,4654809	660,434329
691,2355529	131,4708255	263,5519027	395,5046483	527,2844882	658,830824
719,6193808	130,6526358	262,4368112	393,9874827	525,2222686	656,029172
750,3101325	128,996839	260,1828094	390,9219019	521,0550301	650,365919
779,443986	126,0878508	256,2253146	385,5405393	513,7395032	640,422489
810,0639893	121,6984256	250,2555886	377,4237583	502,7051748	621,578404
840,5846457	92,84028429	218,6758644	343,4194718	466,8902332	588,877256
869,9845724	65,42140976	186,7032241	306,1379014	423,4192349	538,190198
900,1204732	23,87305795	138,2563183	249,6480651	357,5521614	461,390127
930,0745141	0	72,82215897	173,3519386	268,5918127	357,664184
959,5629165	0	0	79,23715594	158,8557077	229,714522
997,1337555	0	0	0	0	34,3560428
1003	0	0	0	0	0

Table 5: Parameters of the Power Subsystem.

Parameters	Abbreviations	Value
Maximum DC bus voltage	V_{DC}	807,4V
Maximum DC current	I_{DC}	627,84A
Link Capacitor	C_{link}	65.000µF
Converter Gain	K_{PWM}	$\frac{2}{3}V_{DC}^{*}$
Switching Frequency	F_{PWM}	24.416Hz
Line Inductance	L	0,15mH
AC system	v_{abc}	- Voltage level: 230V(rms) phase-to-neutral - Frequency: 50Hz

Table 6: Parameters of the Control Subsystem.

Parameters	Abbreviations	Value
Current Crossover frequency for open loop Bode (Band-width)	f_{cI}	610,4Hz
Current Phase Margin	PM_I	63,5°
Cut-off frequency for the reso-nant filter	ω_c	1rad/s
Proportional constant of the PR controller	$\mathbf{k_{p,I\alpha I\beta}}$	**0,0011**
Integral constant of the PR controller	$\mathbf{k_{i,I\alpha I\beta}}$	**0,1**
Voltage Crossover frequency for open loop Bode (Band-width)	f_{cV}	12,208Hz
Voltage Phase Margin	PM_V	63,5°
Proportional constant of the DC bus voltage regulator	$\mathbf{k_{p,Vcc}}$	**3.977,5**
Integral constant of the DC bus voltage regulator	$\mathbf{k_{i,Vcc}}$	**152.110**
Settling time of the PLL	T_{set}	20ms
Damping factor of the PLL	ζ	$\frac{\sqrt{2}}{2}$
Proportional constant of the PI regulator of the PLL	$\mathbf{k_{p,PLL}}$	$\sqrt{2}$
Integral constant of the PI regulator of the PLL	$\mathbf{k_{i,PLL}}$	**325,2691**

Sample period of the Plant	T_s	5,1196µs
Sample period of the Control Subsystem	T_{reg}	40,957µs

4.2 Standards, Procedures, and Methodology

In this project, several **Standards** are used to deal with the connection of the 3-phase PV system to the public utility grid:

1. IEC, “Electromagnetic compatibility (EMC) - Part 2-2: Environment - Compatibility levels for low-frequency conducted disturbances and signalling in public low-voltage power supply systems”, *IEC 61000-2-2*, 2002 [3]. This standard specifies the limits for the odd harmonic distortions of the low voltage utility grid and is shown in Table 6.

Table 7: Odd harmonic distortions of the low voltage utility grid voltages.

Harmonic order h	***Harmonic voltage (%)***
5	6
7	5
11	3,5
13	3
17	2
19	1,5
23	1,5
25	1,5
>25	0,2+1,3*25/h

2. IEEE, “IEEE Recommended practices and requirements for harmonic control in electrical power systems”, *IEEE Std. 519-1992*, 1993 [4]. This standard specifies the limits for the harmonic distortions of the grid currents and is shown in Table 7.

Table 8: Harmonic distortions in % for the grid current.

I_{SC}/I_L	*<11*	*11≤ n <17*	*17≤ n <23*	*23≤ n <35*	*35≤ n*	*THD (%)*
<20	4,0	2,0	1,5	0,6	0,3	5,0
20-50	7,0	3,5	2,5	1,0	0,5	8,0
50-100	10,0	4,5	4,0	1,5	0,7	12,0
100-1.000	12,0	5,5	5,0	2,0	1,0	15,0
>1.000	15,0	7,0	6,0	2,5	1,4	20,0

3. IEC, “Wind turbine generator systems – Part 21: Measurement and assessment of power quality characteristics of grid connected wind turbines”, *IEC 61400-21*, 2001[5]. This standard specifies the LVRT requirements as shown in Figure 13 (a).

Regarding the **Methodology**, the algorithms were tested by using **the Controller-Hardware-in-the-Loop (CHIL**) Simulation technique in which the power subsystem (including the PV Generator, the 3-phase, the inverter, the L filter and the utility grid) were modelled with PLECS tools, meanwhile the control subsystem were modelled using SIMULINK blocks. In both cases the C-codes were generated using the Model-Based design method and downloaded into the Real Time Digital Simulator (RTDS) for the former, and into the real microcontroller for the latter, running both in real time.

4.3 Test Set-up(s)

According to the several features described in Topic 3, the setup was built with two hardware units: the PLECS RT Box 1 [13] working as the Real Time Digital Simulator (RTDS) for the Power subsystem, and the TMS320F28379D Dual-Core Delfino Microcontroller [14] for the Control subsystem. The former is programmed by its own software environment, meanwhile the latter is programmed using MATLAB/SIMULINK in a Model-Based design environment using SIMULINK blocks in order to model the control algorithms. Both units were run in real time and several measurements of the output signals of the corresponding voltages, currents, instantaneous active and reactive powers of the model, among others, were displayed and recorded in the host PC for monitoring purposes. The block diagram of the implemented set-up is depicted in the next Figure, whereas the interface for the analog and digital signals are described in Tables 9 and 10.

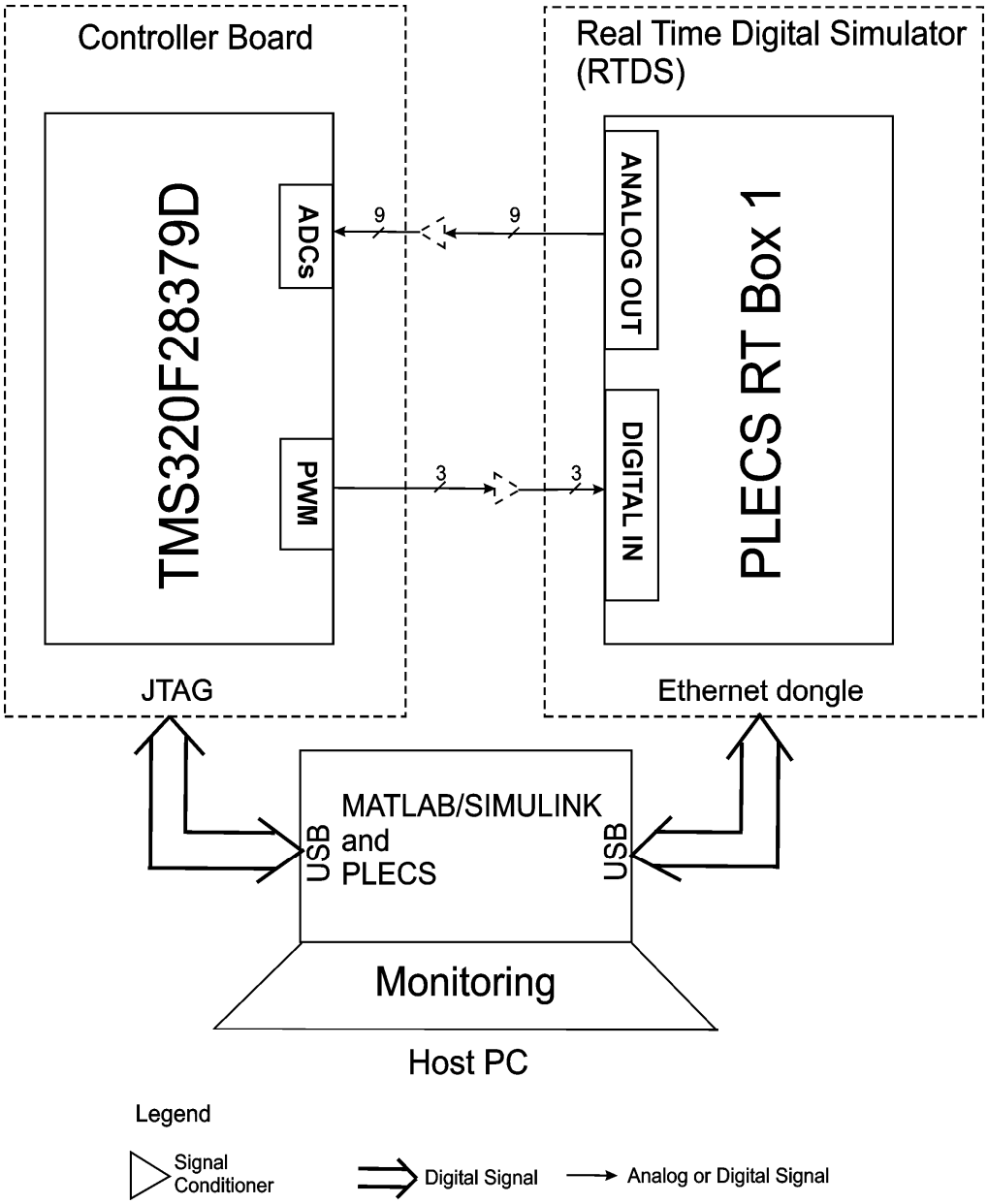

*Figure 6: Block diagram of the **implemented** CHIL Simulation test setup.*

The following Tables show the pinning of the Analog and Digital Signals between the PLECS RT Box 1 and the TMS320F28379D microcontroller:

Table 9: Pinning of the Analog Signals.

PLECS	RT-Box	F28379D	
	A_out 0	DCINA14, CMPIN4P	
	A_out 1	ADCINC3, CMPIN6N	
Vsn	A_out 2	ADCINB3, CMPIN3N	s
Vtn	A_out 3	ADCINA3, CMPIN1N	t
	A_out 4	ADCINC2, CMPIN6P	
Is	A_out 5	ADCINB2, CMPIN3P	
It	A_out 6	ADCINA2, CMPII NOT WORK	
P	A_out 7	ADCINA0 DACa	
	A_out 8	ADCIN15, CMPIN4N	
	A_out 9	ADCINC5, CMPIN5N	
Ir	A_out 10	ADCINB5	
It	A_out 11	ADCINA5, CMPIN2N	
	A_out 12	ADCINC4, CMPIN5P	
Vrn	A_out 13	ADCINB4	r
Vdc	A_out 14	ADCINA4, CMPIN2P	
Idc	A_out 15	ADCINA1 DACb	
	NA	ADCINB1 DACc	

Table 10: Pinning of the Digital Signals.

PLECS		F28379D
	D_in 0	GPIO0, EPWM1A
	D_in 1	GPIO1, EPWM1B
PWM2	D_in 2	GPIO2, EPWM2A, OUT-XBAR1
	D_in 3	GPIO3, EPWM2B, OUT-XBAR2
PWM3	D_in 4	GPIO4, EPWM3A, OUT-XBAR3
	D_in 5	GPIO5, EPWM3B, OUT-XBAR3
	D_in 6	GPIO61, SPISTEA, OUT-XBAR4
	D_in 7	GPIO123
	D_in 8	
	D_in 9	
	D_in 10	
	D_in 11	
	D_in 12	
	D_in 13	
	D_in 14	
	D_in 15	
PWM1	D_in 16	GPIO6, EPWM4A, OUT-XBAR4
	D_in 17	GPIO7, EPWM4B, OUT-XBAR5
	D_in 18	GPIO8, EPWM5A, ADCSO-CAO
	D_in 19	GPIO9, EPWM5B, OUT-XBAR6
	D_in 20	GPIO10, EPWM6A, ADC-SOCBO
	D_in 21	GPIO11, EPWM6B, OUT-XBAR7
	D_in 22	GPIO66, SPISTEB
	D_in 23	GPIO131
	D_in 24	GPIO60, SPICLKA, OUT-XBAR3, SPISIMOB
	D_in 25	GPIO22, EPWM12A, SPI-CLKB
	D_in 26	GPIO105
	D_in 27	GPIO58, SPICLKB, SPISI-MOA, OUTXBAR1
	D_in 28	
	D_in 29	
	D_in 30	
	D_in 31	

5 Results and Conclusions

The following tests were carried out directly using the CHIL Simulation technique using the setup described above. Two Proportional-Resonant (PR) regulators in α-β axes together with the Current References Generator block described in Figure 4 were used to cancel the oscillating components (2ω harmonics, where ω is the nominal angular frequency) in the instantaneous active (P) and/or reactive (Q) powers, or to allow balanced or distorted 3-phase line currents when unbalanced faults occur.

5.1 Positive Sequence Detector + dq PLL (Synchronous Reference Frame PLL) as the synchronization algorithm

The positive- sequence of the 3-phase system $[u_a\ u_b\ u_c]^T$ can be expressed as follows [16]:

$$u_a^+ = \frac{1}{3}u_a - \frac{1}{6}(u_b + u_c) - \frac{1}{2\sqrt{3}\,j}(u_b - u_c) \tag{2}$$

$$u_b^+ = -(u_{a+} + u_{c+})$$

$$u_c^+ = \frac{1}{3}u_c - \frac{1}{6}(u_a + u_b) - \frac{1}{2\sqrt{3}\,j}(u_a - u_b)$$

where the operator 1/j (named S90) can be designed with the following transfer function:

$$H_{S90}(s) = \frac{1 - \frac{s}{\omega_o}}{1 + \frac{s}{\omega_o}} \tag{3}$$

with unity gain at all frequencies and a phase of -90° at the nominal frequency ω_o.

For the inverter-grid synchronization, the positive sequence of the phase angle θ of the grid voltage vector $\mathbf{u_{AC}}$ is calculated, and a Positive Sequence Detector (PSD) is added to reject the negative sequence of the 3-phase utility grid voltages during unbalances [16,17]. Figure 7 depicts a synchronization scheme using the PSD mentioned above and a PLL for 3-phase systems [18], known as dq PLL. The quadrature component v^+_q of the 3-phase utility grid voltages is fed to a PI regulator whose output reduces the value of v^+_q to zero. The output of the PI regulator plus an initial value of the angular speed ω_{offset} (added to reduce the time to track the phase angle θ and improve the PLL stability) is the positive sequence of the angular speed ω^+ of the grid voltage $\mathbf{u_{AC}}$. Finally, an integrator computes the phase angle θ^+.

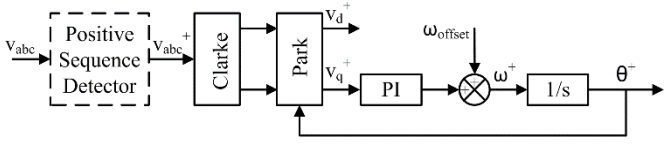

Figure 7: Block diagram of the PSD+dq PLL.

In 5.1.6 a more detailed explanation of the symmetrical components [19] will be done when the LVRT experiments are described.

5.1.1 **Experiment 1.** Harmonic Distortion in the Utility Grid Voltages and constant I_{DC} and V_{DC} at the input of the inverter.

This experiment was carried out to test the setup getting familiar with the simulation environment of the PLECS RT Box1, as well as the debugging tools with the Model-based Design approach using the SIMULINK blocks to build the models of the control algorithms, compile it, generate its C code and download it into the TMS320F28379D microcontroller target.

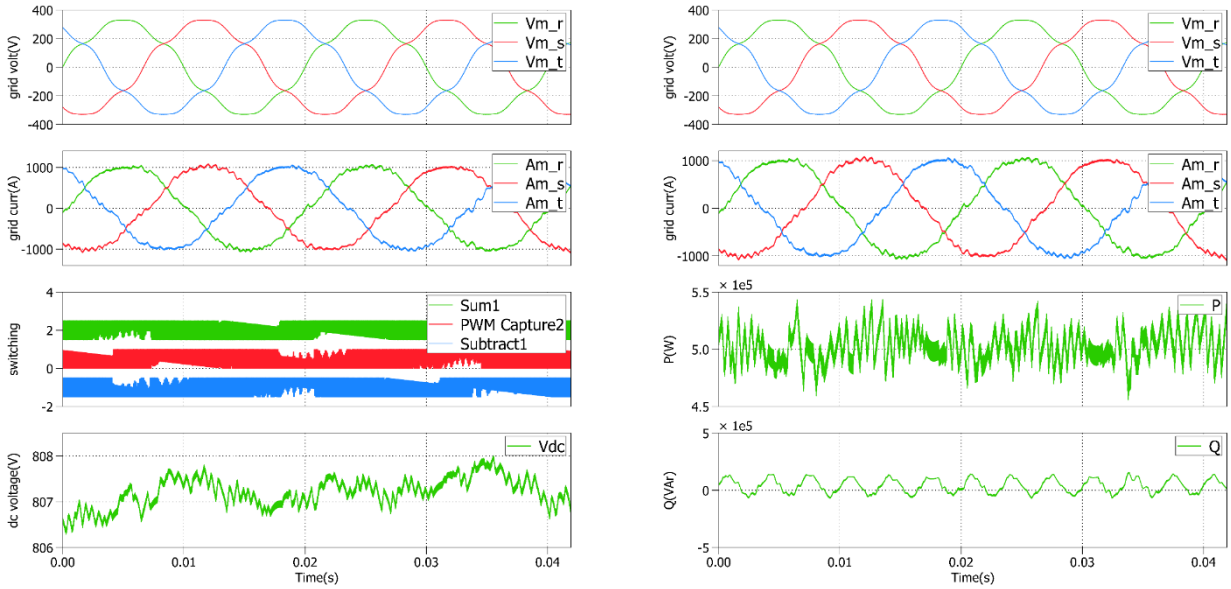

Figure 8: Time evolution of the grid voltages, grid currents, commutation of the 3-phase upper power switches of the inverter, dc bus voltage, instantaneous active (P) and reactive (Q) powers.

As can be seen in the previous Figure, the grid currents in the innermost loop are properly controlled and the distortion harmonics in the 3-phase utility grid voltages are almost cancelled, as well as the DC bus voltage in the outermost loop. For this experiment, the instantaneous active power (P) is around its maximum nominal value of 500kW, meanwhile the instantaneous reactive power (Q) is zero for unity power factor operation as Tables 3 and 4 show. The displayed commutation of the 3-phase upper power switches close the overall control loops and demonstrate the proper behaviour of the VSI module.

5.1.2 **Experiment 2.** Voltage sag of 30% in phase 3 (constant I_{DC} and V_{DC} at the input of the inverter and **no positive sequence detector** is used).

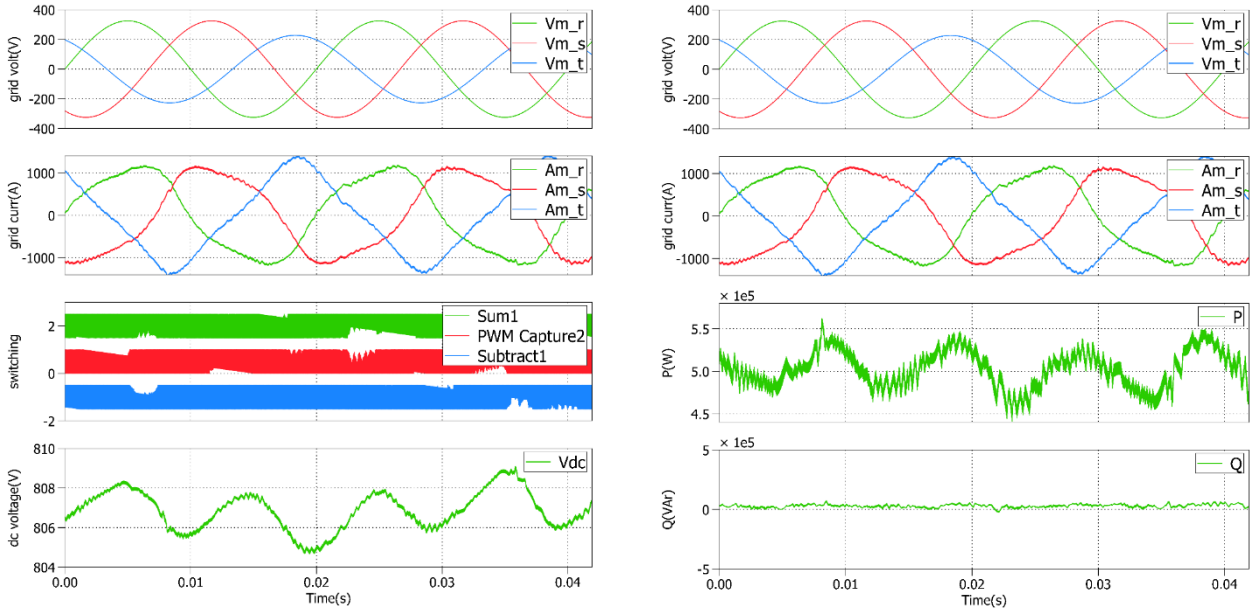

(a) (b)

Figure 9: Time evolution of the grid voltages, grid currents, commutation, dc bus voltage, instantaneous active (P) and reactive (Q) powers. No positive sequence detector (PSD) is used.

In this experiment, the 3-phase grid currents are completed distorted because there is no control over the negative- sequence of the 3-phase grid voltages that are feedback into the innermost current loop [7], and produces the second order harmonics 2ω throughout the system, i.e. in the DC bus voltage and in the instantaneous active power (P). However, the mean values of P and Q are 500kW and zero, respectively, yielding a unity power factor operation.

5.1.3 **Experiment 3.** Voltage sag of 30% in phase 3 (constant I_{DC} and V_{DC} at the input of the inverter and a **positive sequence detector** is used).

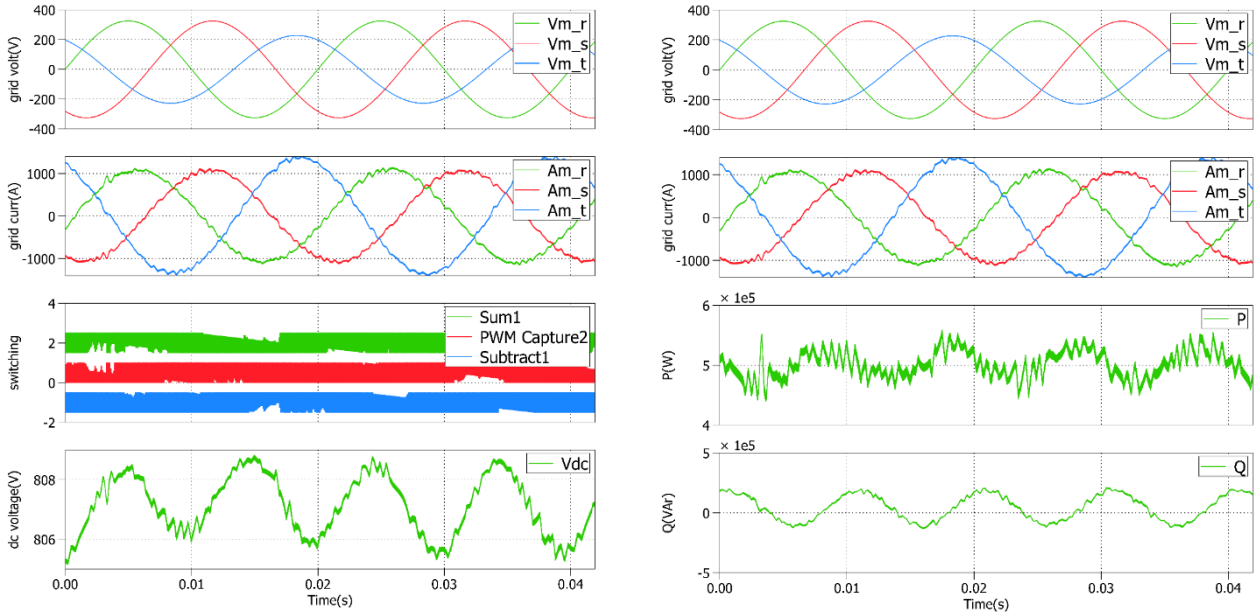

(a) (b)

Figure 10: Time evolution of the grid voltages, grid currents, commutation, dc bus voltage, instantaneous active (P) and reactive (Q) powers. A positive sequence detector (PSD) is used.

In this experiment, the 3-phase currents are not distorted because the detection of the positive-sequence of the 3-phase grid voltages avoids the feedback of its negative- sequence into the inner-most current loop [7]. However, the second order harmonics 2ω also appears in the DC bus voltage, the instantaneous active (P) and reactive (Q) powers. Again P and Q have a mean value around 500kW and zero, respectively for unity power factor operation.

5.1.4 Experiment 4. A perturb & Observe MPPT algorithm is employ with the maximum constant irradiance of 1000 W/m^2.

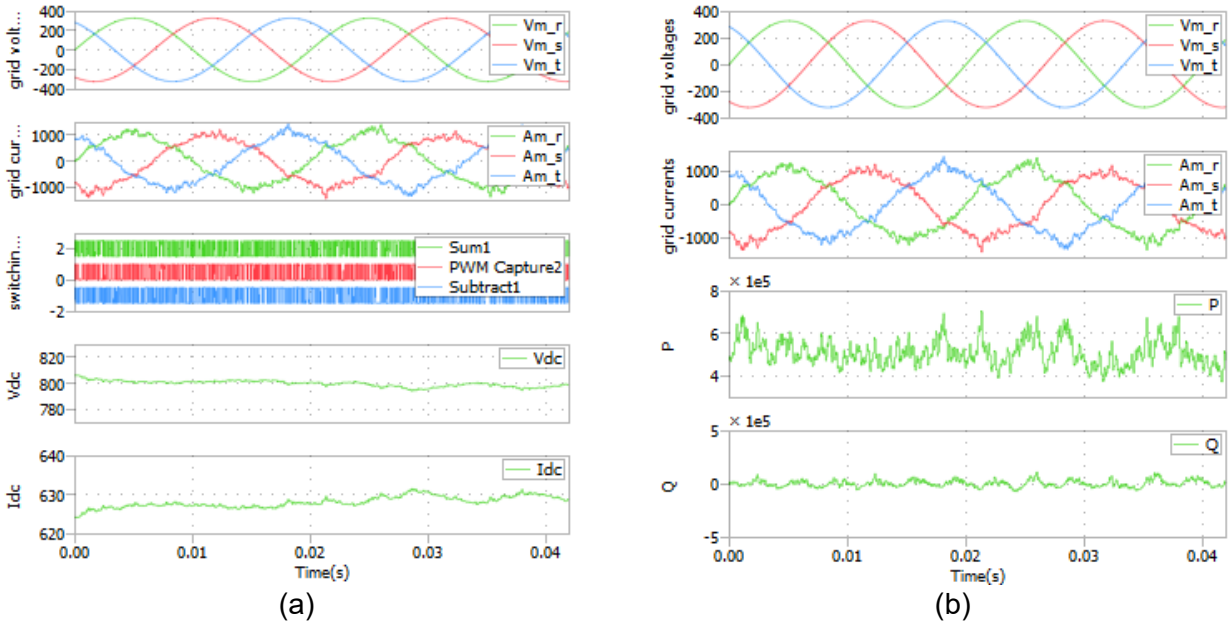

Figure 11: Time evolution of the grid voltages, grid currents, commutation, dc bus voltage, dc current, instantaneous active (P) and reactive (Q) powers.

As can be seen in this experiment, the MPPT algorithm computes the DC bus voltage reference command for the outermost voltage loop. So, a DC bus voltage and current around 800V and 625A are attained, respectively, according to Tables 3 and 4, feeding an instantaneous active (P) and reactive (Q) powers of 500kW and zero, respectively.

5.1.5 Experiment 5. A perturb & Observe MPPT algorithm is employ with an irradiance step from 800 to 1000W/m^2.

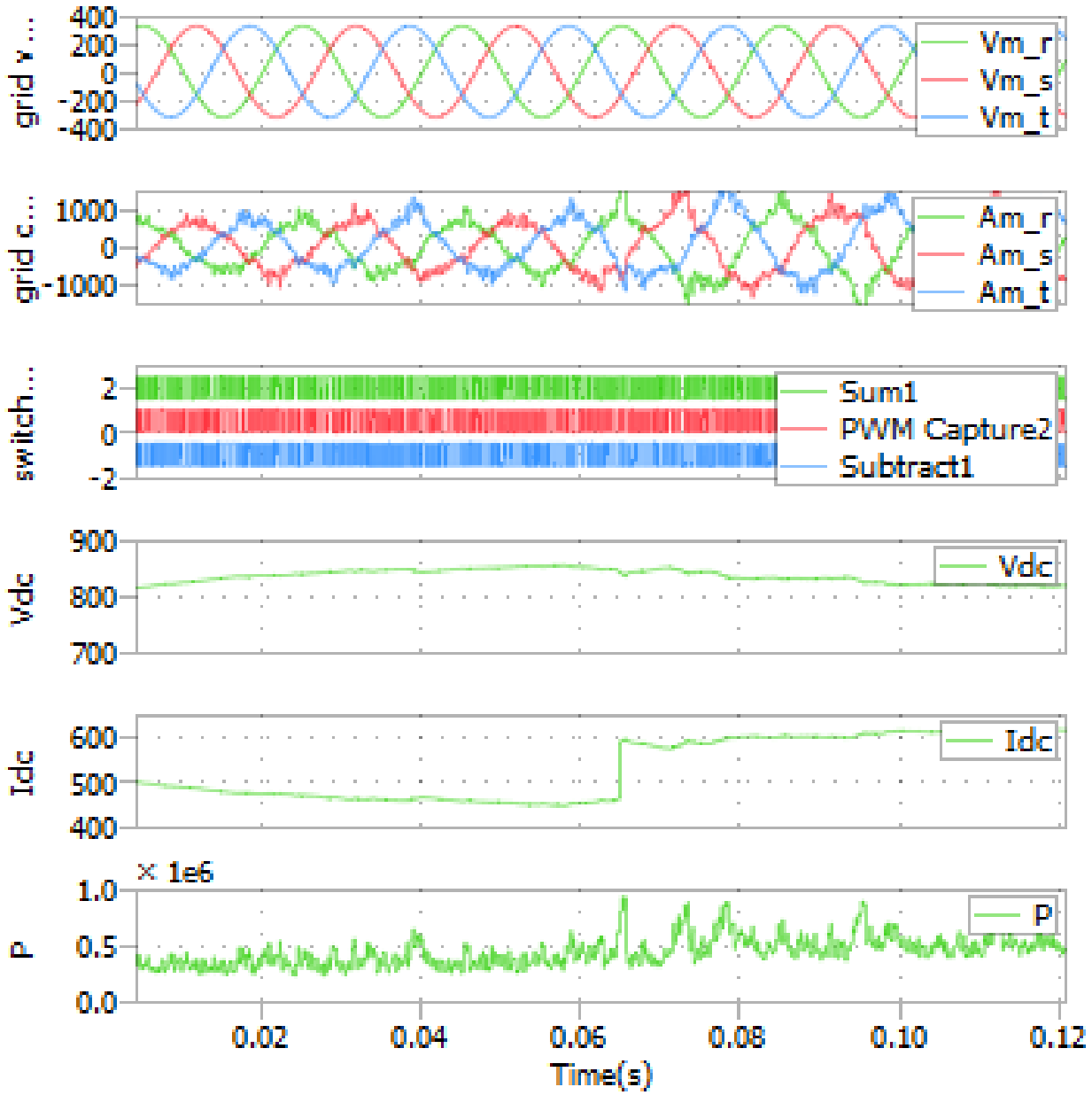

Figure 12: Time evolution of the grid voltages, grid currents, commutation, dc bus voltage, dc current, instantaneous active (P) power.

In this experiment an irradiance step is exerted around 0.065s in the DC current, keeping constant the DC bus voltage. As can be seen, the amplitude of the 3-phase currents increases in order to increase the instantaneous active power (P) fed into the utility grid.

5.1.6 Experiment 6. Low-voltage-ride-through tests are shown for different voltage sags (**no constant** DC bus voltage).

For the implementation of the LVRT capability, the positive- and negative- sequences of the 3-phase utility grid voltages must be calculated using the symmetrical components theory. In general, given a 3-phase system $[u_a\ u_b\ u_c]^T$, the computation of its zero-, positive- and negative- sequences $[u_0\ u_+\ u_-]^T$ of phase *a* is [19]:

$$\begin{bmatrix} u_o \\ u_+ \\ u_- \end{bmatrix} = \frac{1}{3}\begin{bmatrix} 1 & 1 & 1 \\ 1 & a & a^2 \\ 1 & a^2 & a \end{bmatrix}\begin{bmatrix} u_a \\ u_b \\ u_c \end{bmatrix} \tag{4}$$

where $a=e^{j(2\pi/3)}$

The positive- and negative- sequences of the 3-phase system can be expressed as follows [7]:

$$\begin{aligned} u_a^+ &= \frac{1}{3}u_a - \frac{1}{6}(u_b + u_c) - \frac{1}{2\sqrt{3}\,j}(u_b - u_c) \\ u_b^+ &= -(u_{a+} + u_{c+}) \\ u_c^+ &= \frac{1}{3}u_c - \frac{1}{6}(u_a + u_b) - \frac{1}{2\sqrt{3}\,j}(u_a - u_b) \end{aligned} \tag{5}$$

$$\begin{aligned} u_a^- &= \frac{1}{3}u_a - \frac{1}{6}(u_b + u_c) + \frac{1}{2\sqrt{3}\,j}(u_b - u_c) \\ u_b^- &= -(u_{a-} + u_{c-}) \\ u_c^- &= \frac{1}{3}u_c - \frac{1}{6}(u_a + u_b) + \frac{1}{2\sqrt{3}\,j}(u_a - u_b) \end{aligned} \tag{6}$$

For the implementation of eq. (5) and (6), the 1/j operator (named S90) can also be design with eq. (3).

The implementation of the LVRT capability is carried out in this project using two Proportional-Resonant (PR) regulators in α-β axes in order to cancel the oscillating components in the instantaneous active power (P) when unbalanced faults occur. It is worth noting that S90 operator of the PNSD is tuned to the fundamental nominal frequency and is very sensitive to its variation which decreases the power factor of the grid-connected inverter. To avoid the power factor degradation when the nominal frequency varies, enhance structures with adaptive filters must be used, i.e. the DSOGI-FLL and the MSOGI-FLL [19].

Figure 13 (a) and (b) depict the LVRT requirements according to IEC 61400-21 [5,15] and the reactive power to be injected into the utility grid according the depth of the voltage sag in Spain [6], respectively. One of the steps to be able to implement the LVRT capability is to quickly detect the voltage sag through the calculation of the value of V_{gf} by measuring the 3-phase utility grid voltages,

extracting its positive- sequence and normalizing with the amplitude of the 3-phase utility grid line-to-line voltages (see eq. (7)) [6]. The depth of the voltage sag according to IEC 61400-21 is limited to a value of V_{gf} bellow 0.85 in order to consider that a voltage sag has occurred; the value of the maximum apparent power S_{max} will be calculated using the positive- and negative- sequences of the 3-phase utility grid voltages and the nominal apparent power S_{nom}, normalizing again with the amplitude of the 3-phase utility grid line-to-line voltages (eq. 8) [6].

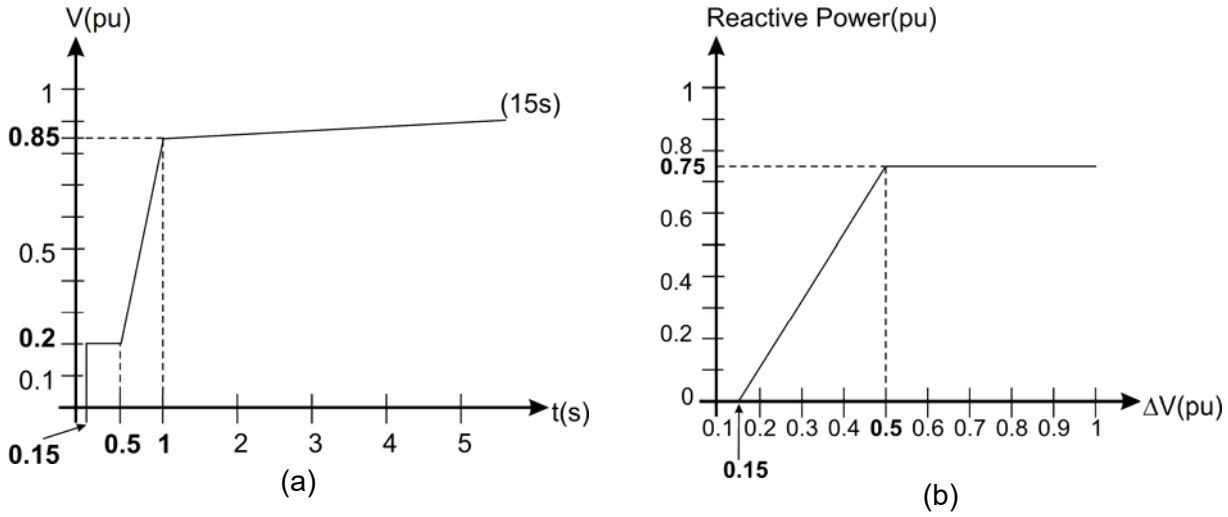

Figure 13: (a) LVRT requirements according to IEC 61400-21.
(b) Reactive power to be injected into the grid during voltage sags in Spain.

$$V_{gf} = \frac{\sqrt{v_{\alpha}^{+2} + v_{\beta}^{+2}}}{v_{nom(line-to-line)}} \tag{7}$$

where V_{gf} is the depth of the voltage sag.

$$S_{\max} = \frac{\sqrt{v_{\alpha}^{+2} + v_{\beta}^{+2}} - \sqrt{v_{\alpha}^{-2} + v_{\beta}^{-2}}}{v_{nom(line-to-line)}} S_{nom} \tag{8}$$

where S_{max} is the maximum apparent power during the voltage sag and the nominal apparent power S_{nom} is around 507kW (DC output power of the PV Generator as seen in Table 3).

Figure 14 depicts the flowchart for the implementation of the LVRT capability of the grid-connected inverter during voltage sags.

If $V_{gf} \geq 0.85$, no fault is detected and a normal operation is achieved with no instantaneous reactive power injected into the grid (Q*= 0 for unity power factor operation) as shown in Figure 13 (b), and allowing the application of the maximum power point tracking (MPPT) algorithm. In this case, the maximum available power at the input of the PV Generator is delivered to the utility grid for a given irradiance and temperature, and the output of the MPPT module is the DC voltage reference command V_{DC}^{*} MPP for the outer voltage control loop which corresponds to the maximum instantaneous active power (P*) as shown in Figure 15.

On the contrary, if V_{gf} < 0.85, the “Fault Signal” flag is activated. Firstly, the duration of the voltage sag is measured and if it is higher than the one specified in Figure 13 (a), the inverter is disconnected from the utility grid; if not, the values of Q and P_{max} are calculated according to eq. (9) and (10), respectively. Finally, a comparison between P_{max} and P* is done in order to activate the MPPT or the non-MPPT algorithms as shown at the bottom left of Figure 14. For the latter, P_{max} is delivered to the grid as shown in Figure 15.

$$\begin{cases} Q = 0, & V_{gf} \geq 0,85 \\ Q = \frac{15}{7} S_{nom}(0,85 - V_{gf}), & 0,5 \leq V_{gf} < 0,85 \\ Q = \frac{3}{4} S_{nom}, & V_{gf} < 0,5 \end{cases} \quad (9)$$

$$P_{\max} = \sqrt{S_{\max}^2 - Q^2} \quad (10)$$

Figure 15 depicts the PV curve operating with MPPT and non-MPPT algorithms for no fault and faulty operations, respectively. It is clear that during the fault the amplitude of the positive- sequence of the 3-phase utility grid voltages decreases and the outer DC voltage controller will try to increase the amplitude of the output inverter currents so as to be able to do the power balance between the PV Generator and the grid for MPP operation. However, due to the current limitation imposed by the Grid Code, the non-MPP operation mode is activated assuring the proper balance of power when voltage sags occur because the output voltage of the PV Generator will move to the right in the PV curve (from (V_{DC}* MPP, P*) to (V_{DC}* non-MPP, P_{max}).

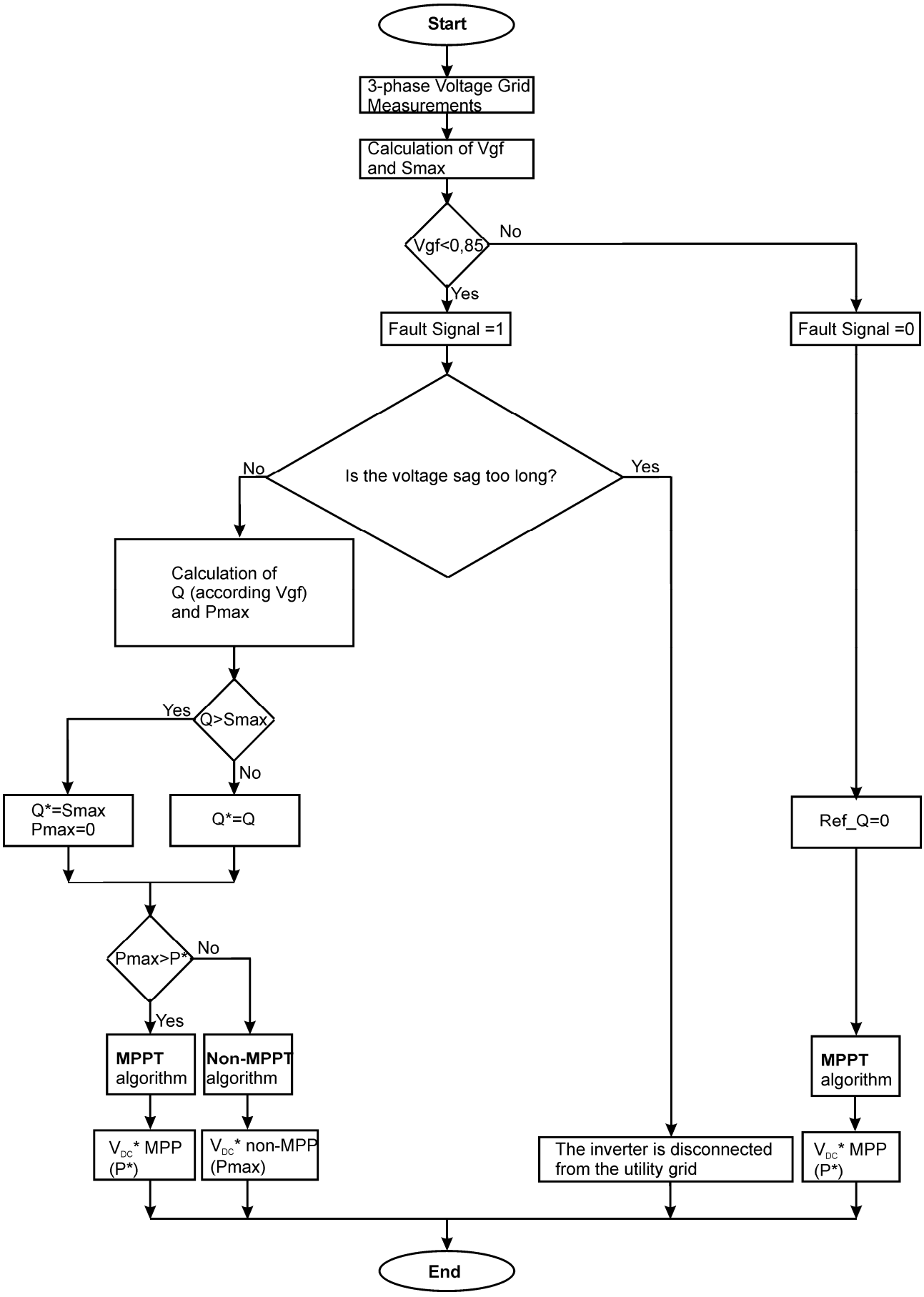

Figure 14: Flowchart of the LVRT algorithm.

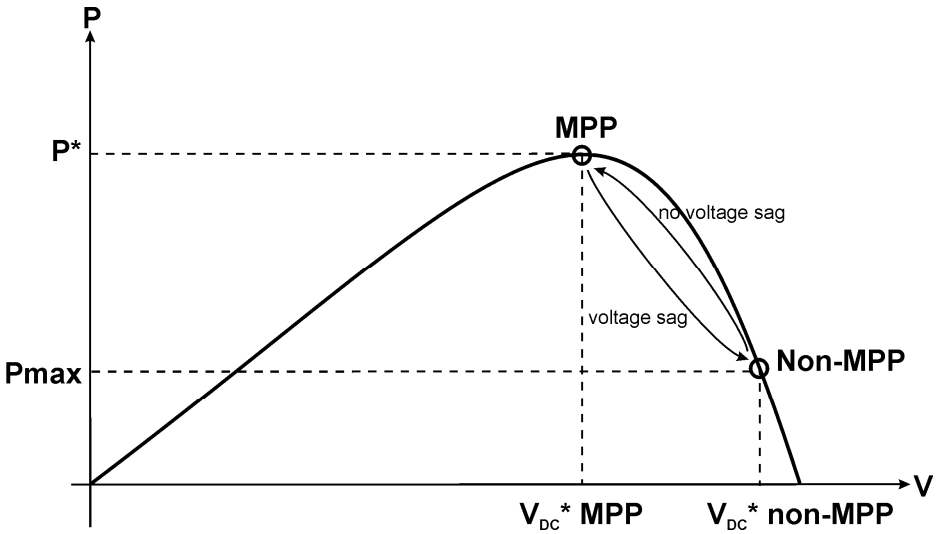

Figure 15: PV curve for MPP and non-MPP.

In the next Figures, some tests are shown to demonstrate the LVRT capability when different kind of voltage sags occur at different irradiances. The time evolution of the DC bus voltage and current at the output of the PV Generator, the 3-phase grid voltages and currents at the grid side, and the instantaneous active (P) and reactive (Q) powers delivered to the utility grid are shown in (a), meanwhile the same variables are depicted during the voltage sags in (b).

In all the tests, the maximum power point (MPP) of the PV Generator is tracked when there is no voltage sags and the $\mathbf{V_{DC}^*MPP}$ DC bus voltage command is applied to the control algorithm to do the power balanced, whereas a zero reactive power operation is attained. However, there is an increment in the DC bus voltage during the voltage sag because the limitation in the amplitude of the line currents to its nominal value (imposed by the Grid Code) decreases the instantaneous active power (P) delivered to the utility grid and a $\mathbf{V_{DC}^*non\text{-}MPP}$ DC bus voltage command is set in this situation (see Figure 15); at the same time some reactive power (Q) is needed according to eq. (9) in order to improve the profile of the utility grid voltages during the sags.

According to the depth of the voltage sag and whether it is a 3-phase or 1-phase event, different behaviour is expected in the controlled variables according the flowchart described in Figure 14. For example, on one hand a 3-phase deep balanced voltage sag (0.1(pu)), G=1000W/m^2, appears in Figure 16 and so, a certain amount of reactive power and zero active power are delivered to the utility grid, with balanced sinusoidal 3-phase grid currents, as can be seen in (b). On the other hand, a moderate voltage sag in phase 3 (0.5(pu)), G=1000W/m^2, appears in Figure 22 and then some instantaneous active and reactive powers are delivered to the utility grid. P is almost a constant value different from zero, meanwhile Q has an oscillation with the second harmonics 2ω (with almost zero mean value), as well as the DC voltage and current; however the 3-phase grid currents are unbalanced sinusoidal (not distorted) as can be seen in (b).

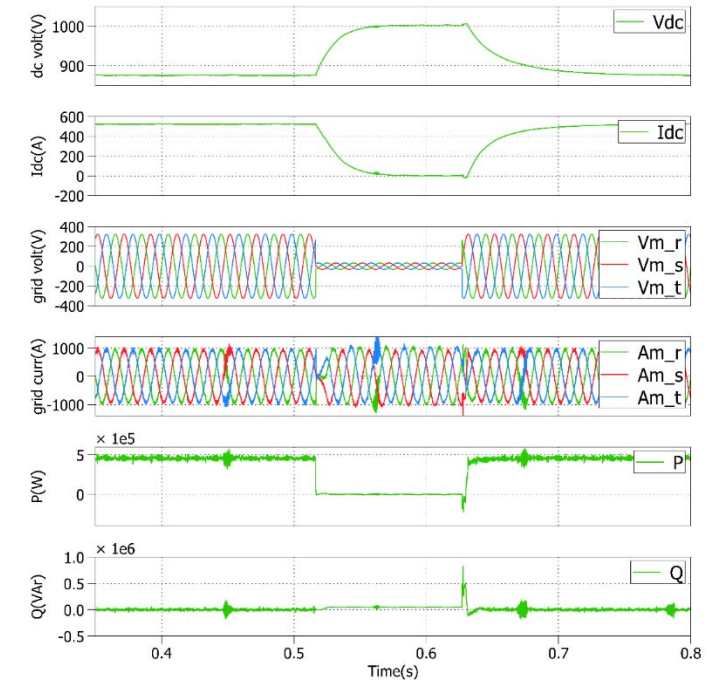

(a)

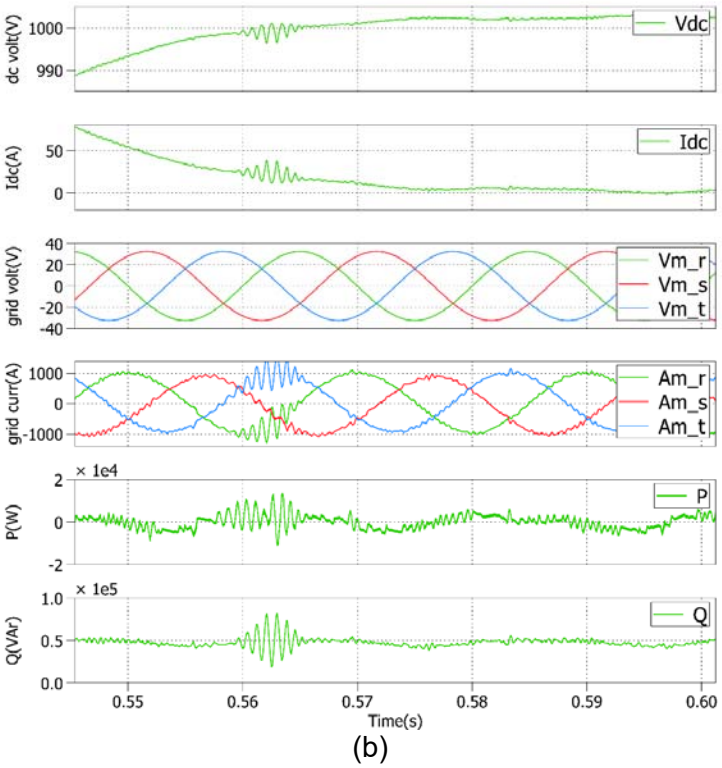

(b)

Figure 16: 3-phase deep voltage sag (0.1 (pu)), G=1000W/m^2.

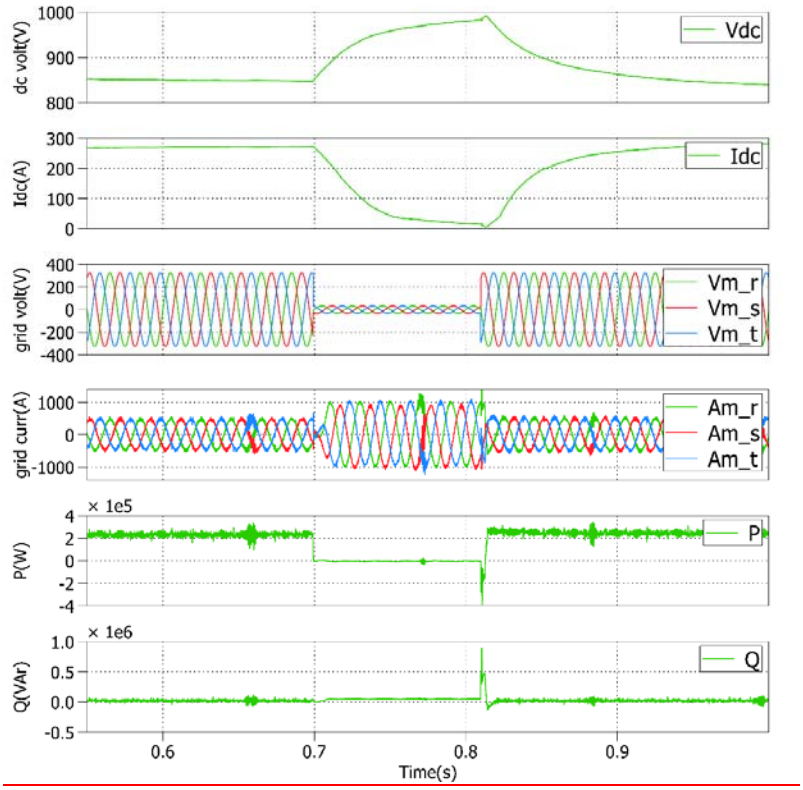

(a)

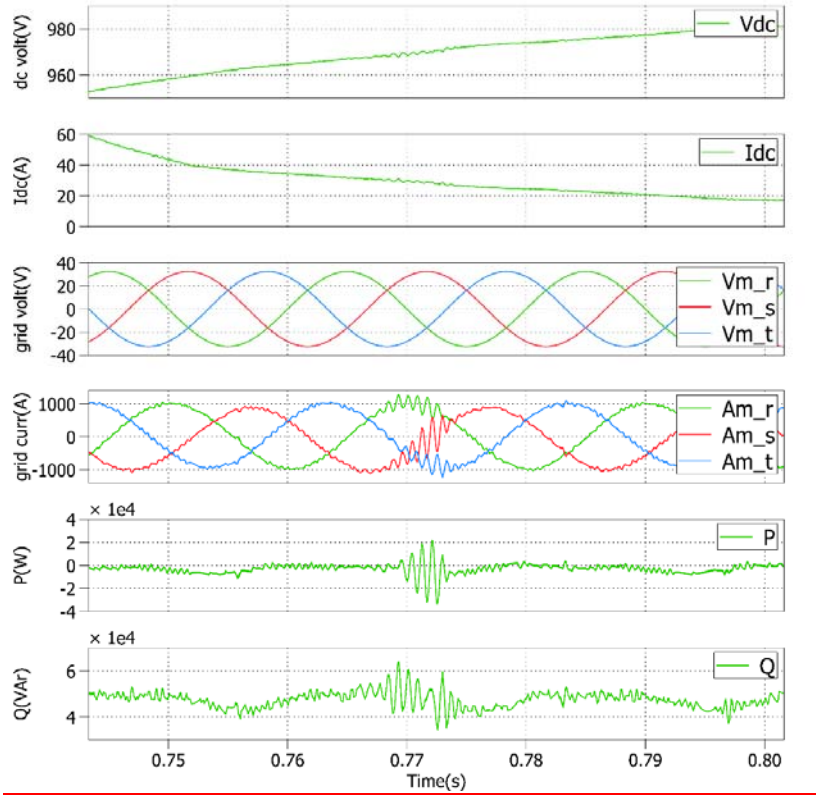

(b)

Figure 17: 3-phase deep voltage sag (0.1 (pu)), G=500W/m^2.

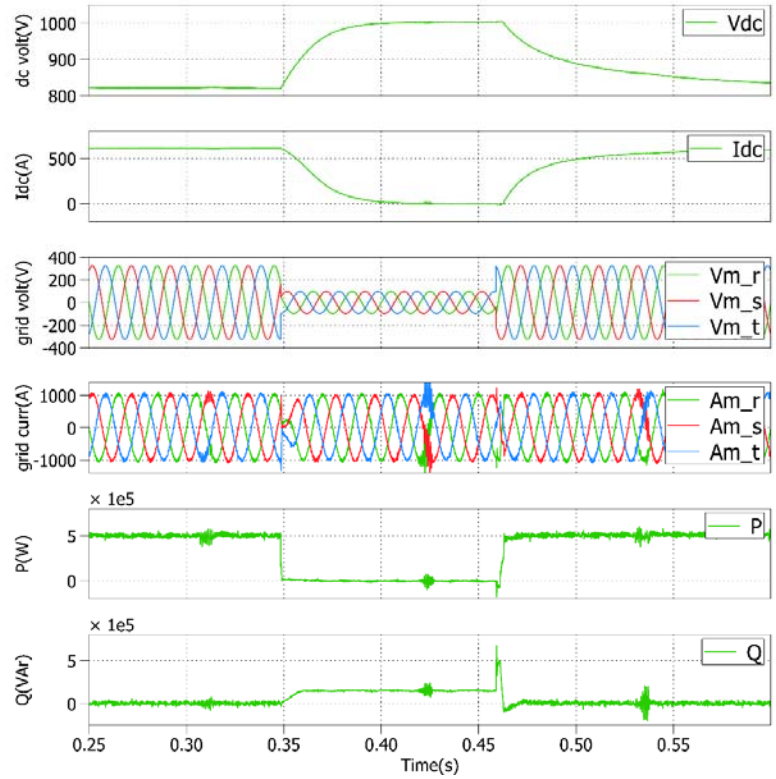

(a)

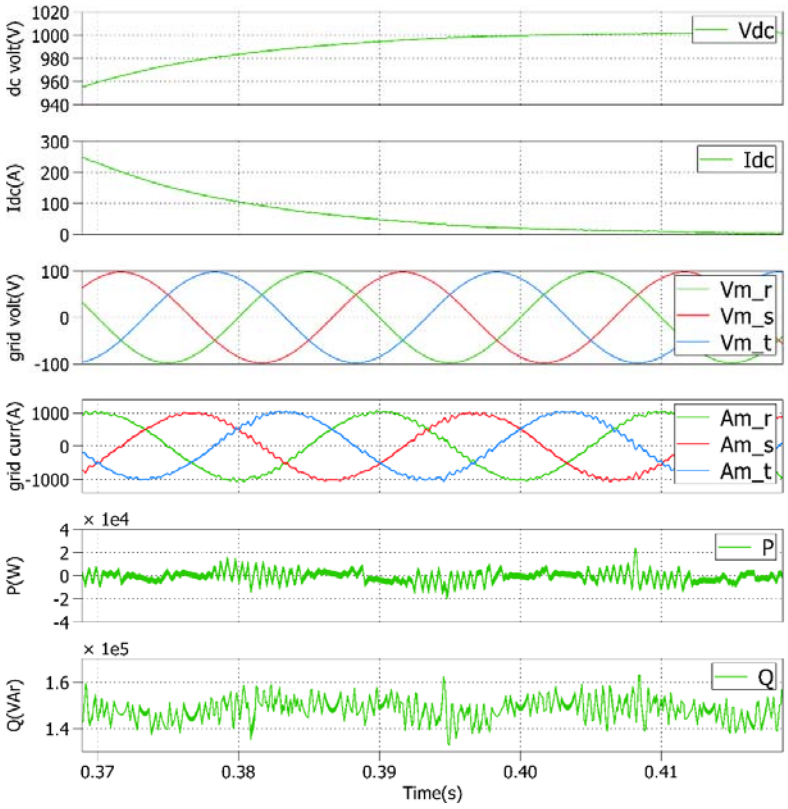

(b)

Figure 18: 3-phase deep voltage sag (0.3 (pu)), G=1000W/m^2.

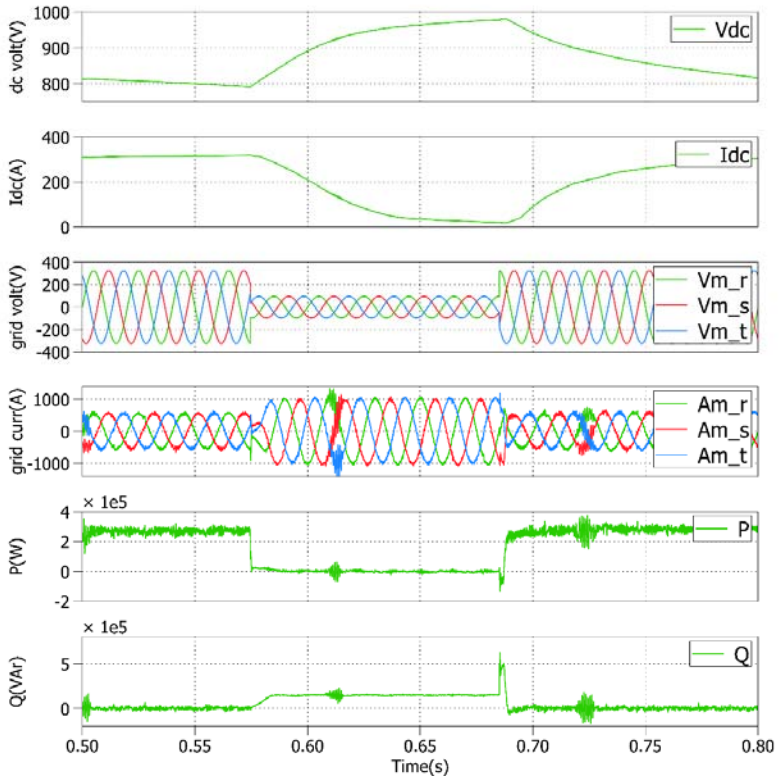

(a)

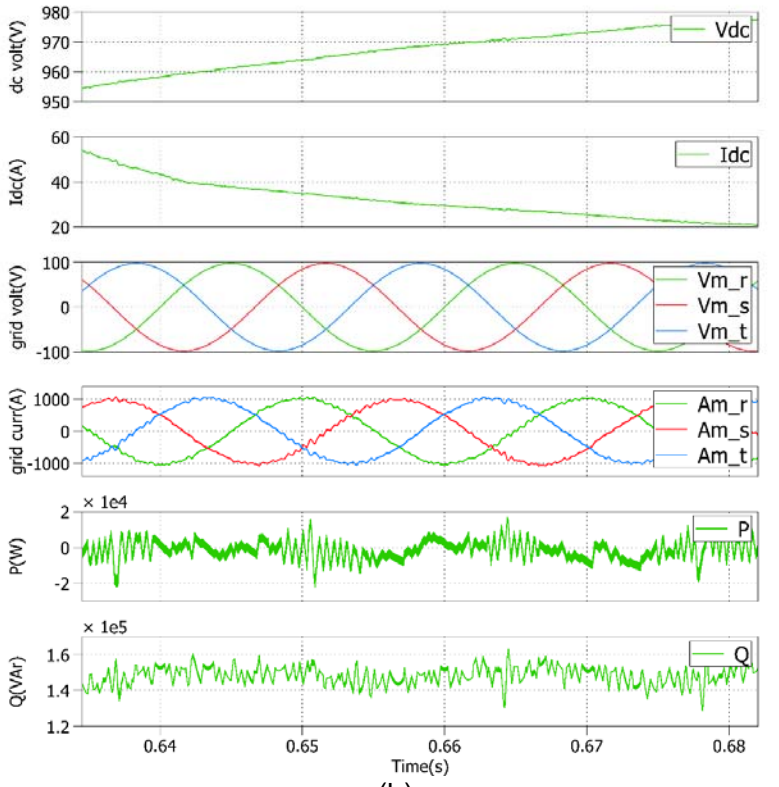

(b)

Figure 19: 3-phase deep voltage sag (0.3 (pu)), G=500W/m².

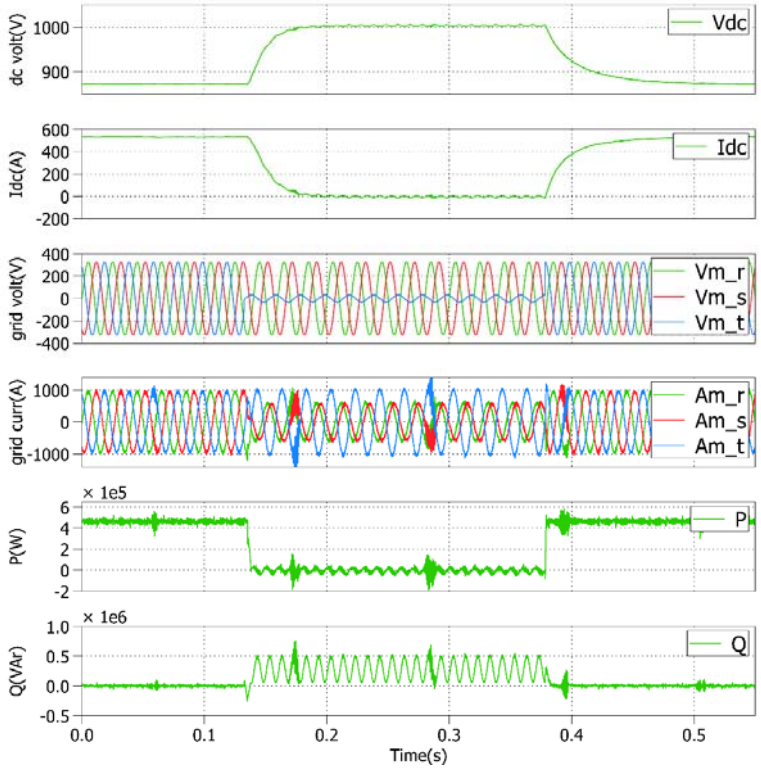

(a)

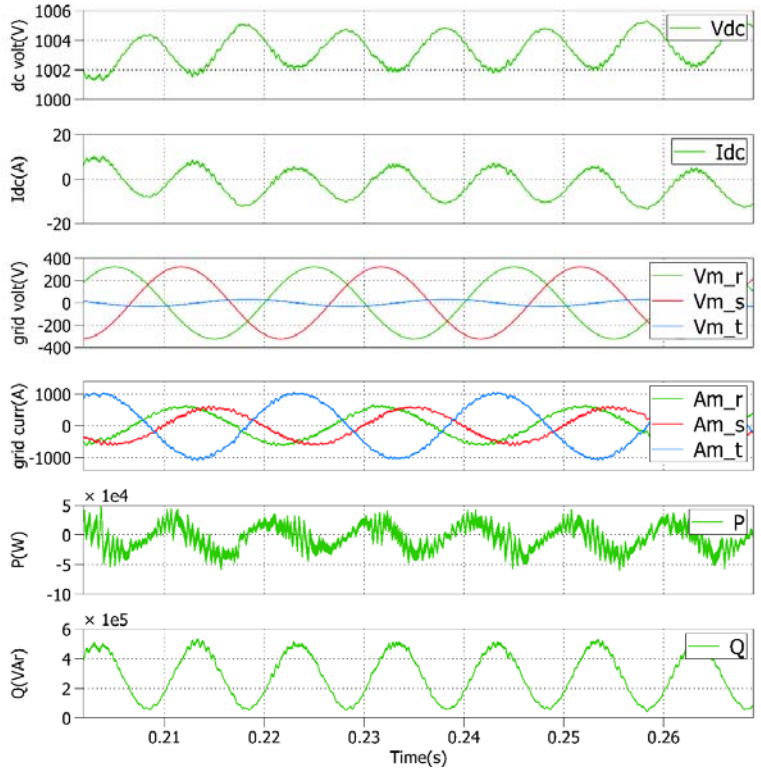

(b)

Figure 20: Deep voltage sag in phase 3 (0.1 (pu)), G=1000W/m^2.

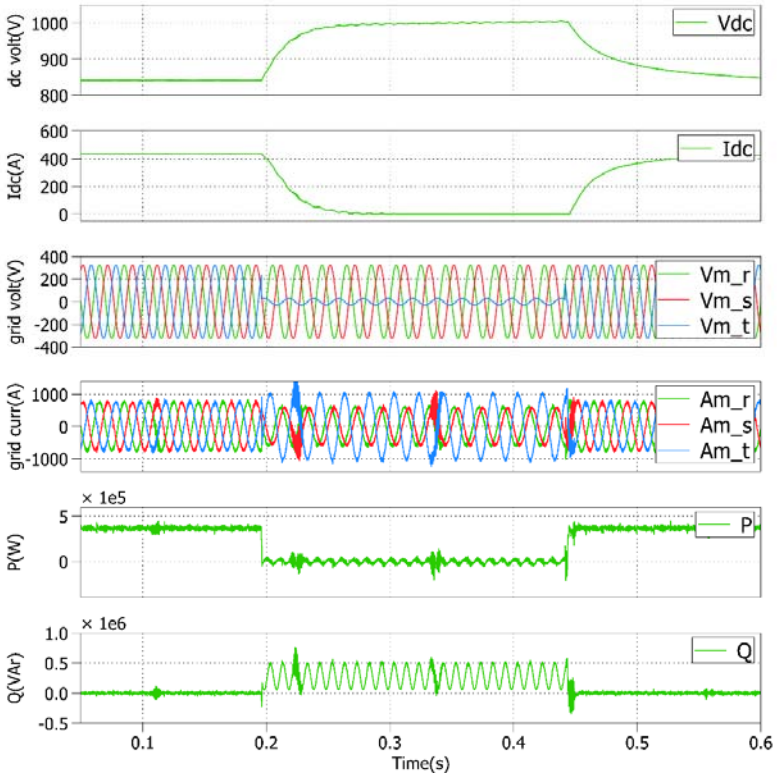

(a)

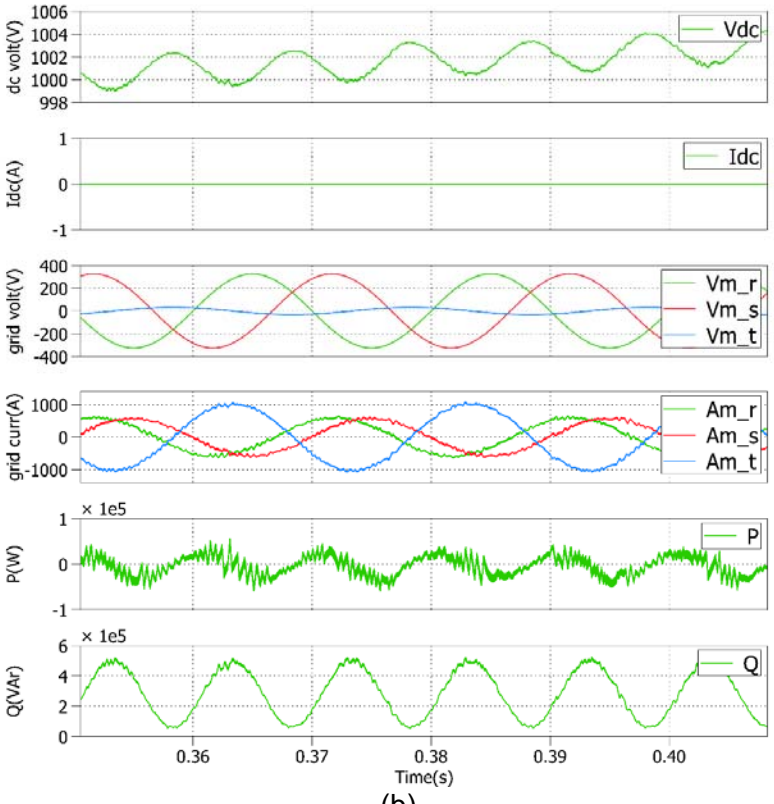

(b)

Figure 21: Deep voltage sag in phase 3 (0.1 (pu)), G=750W/m^2.

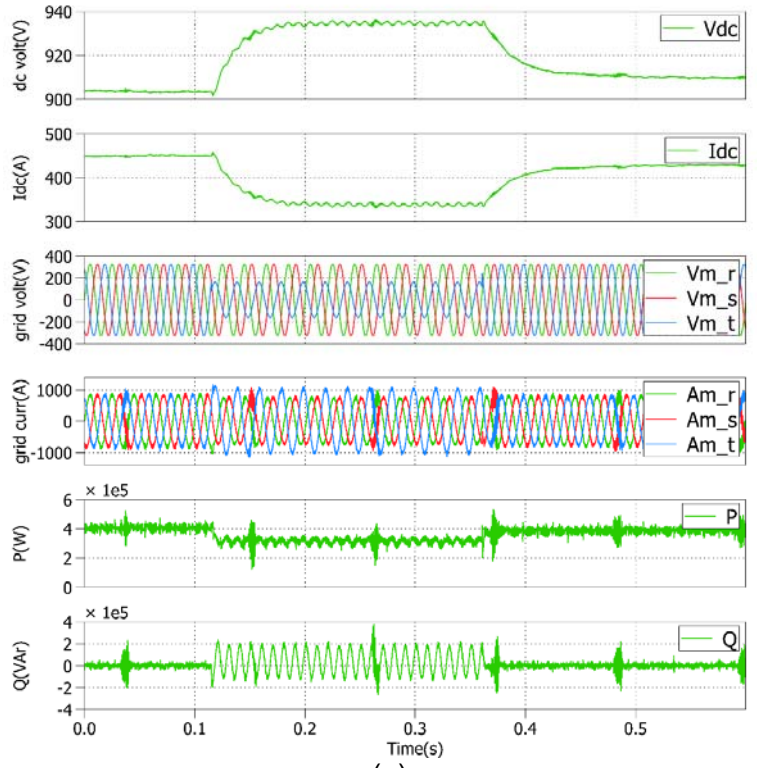

(a)

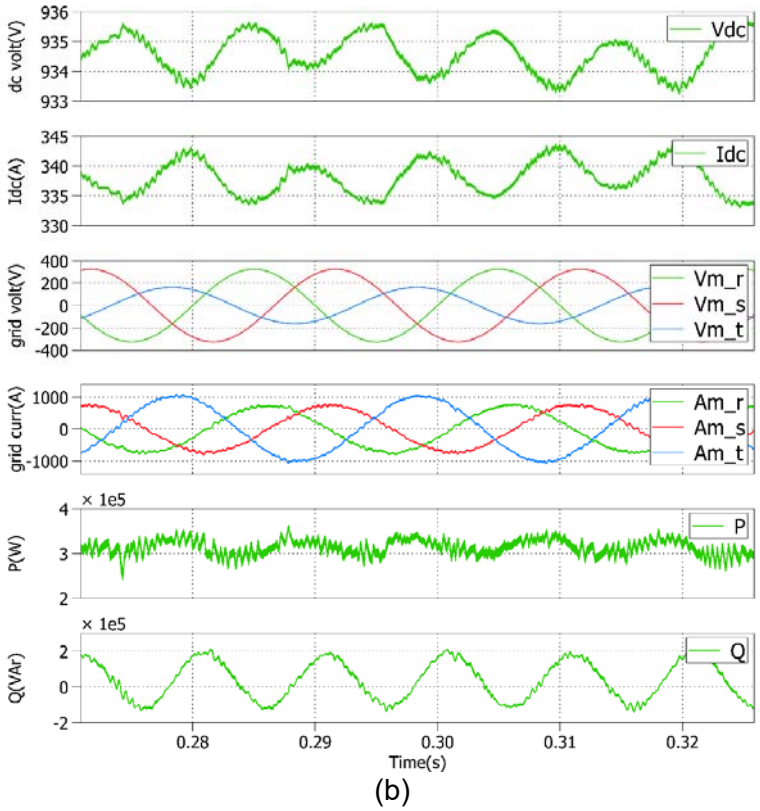

(b)

Figure 22: Moderate voltage sag in phase 3 (0.5 (pu)), G=1000W/m^2.

5.1.7 Experiment 7. Low-voltage-ride-through tests are shown for different voltage sags (**constant** DC bus voltage).

Following, some tests are carried out if a **two-stage system** were used (a DC/DC boost converter is placed between the PV Generator and the 3-phase inverter). In this case, the DC bus voltage at the input of the inverter can be kept constant, whereas the current control of the DC/DC boost converter will do the power balance between the PV Generator and the utility grid. It must be pointed out that the simulation of the DC/DC boost converter is out of the scope of this project.

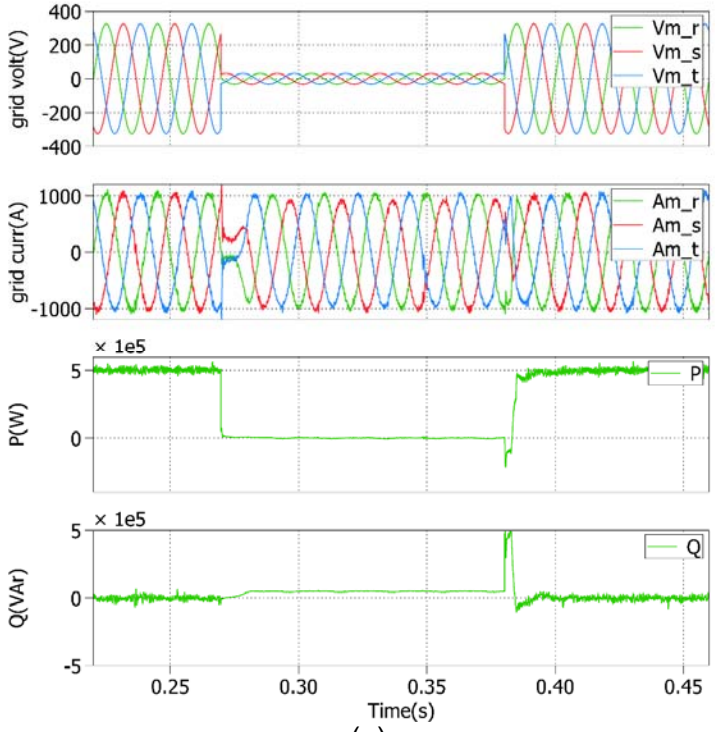

(a)

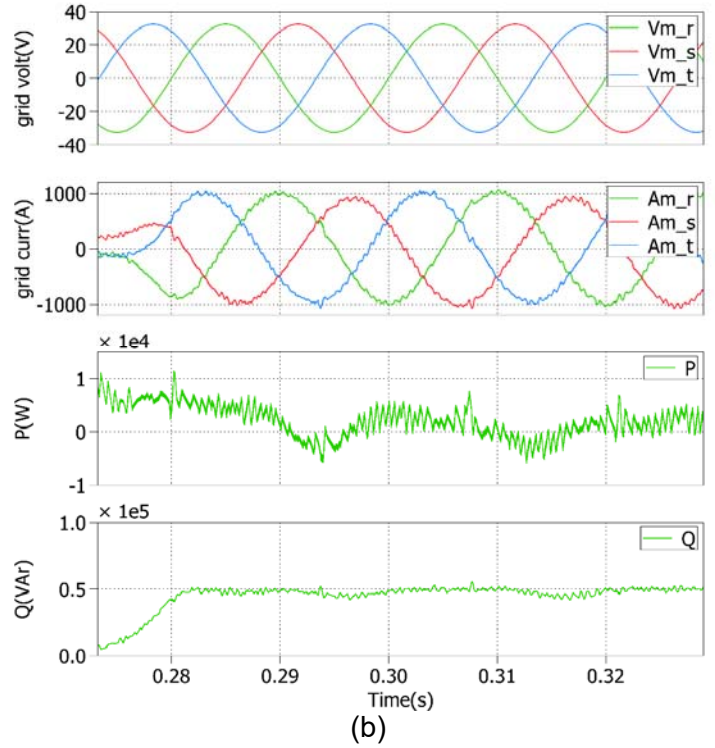

(b)

Figure 23: 3-phase deep voltage sag (0.1 (pu)), G=1000W/m².

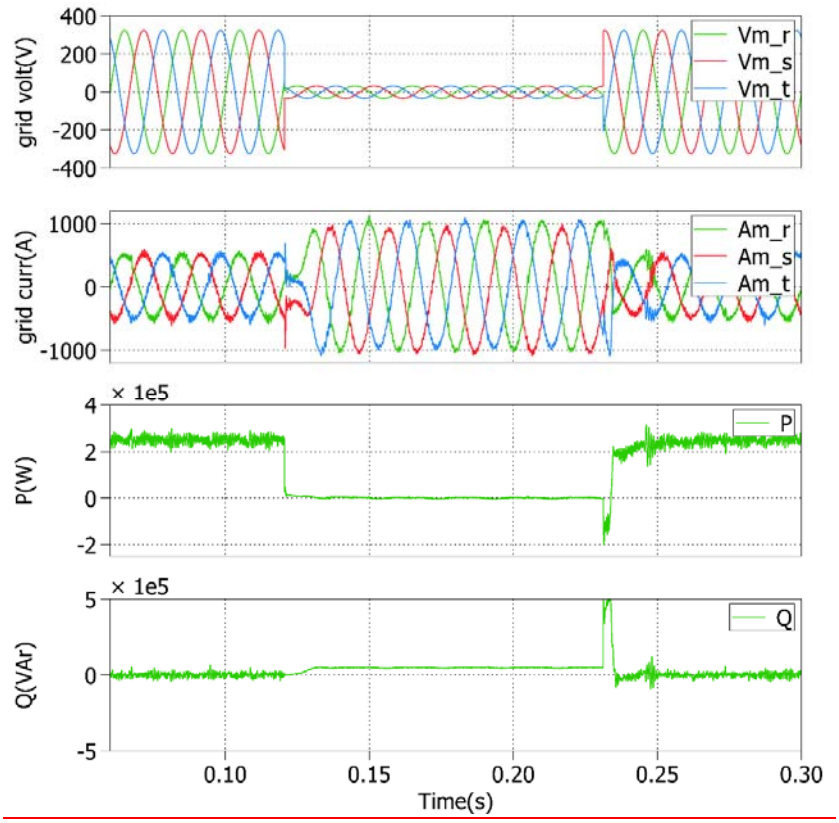

(a)

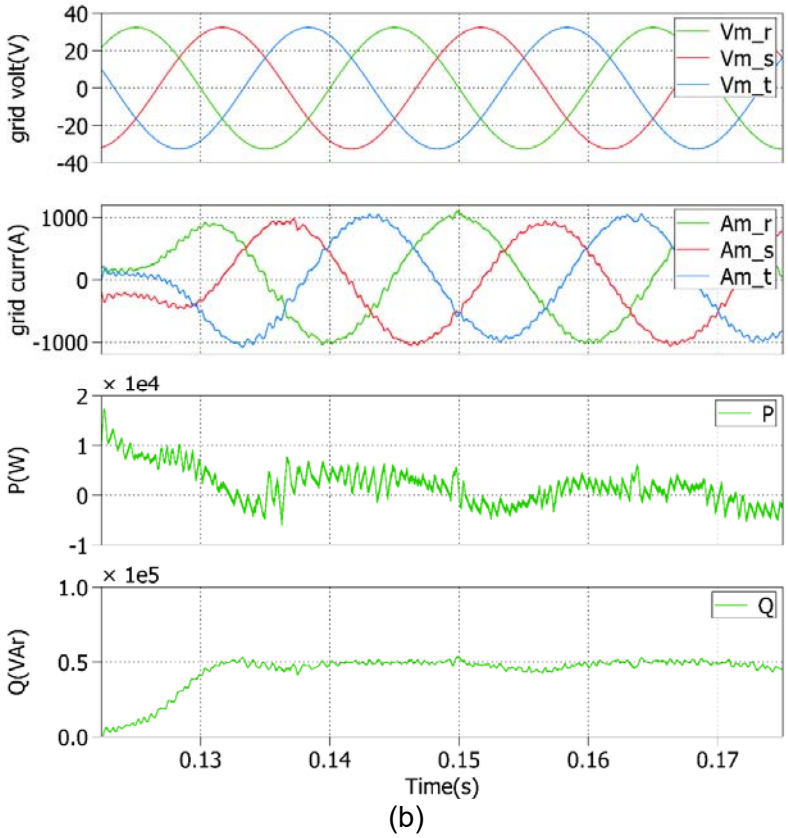

(b)

Figure 24: 3-phase deep voltage sag (0.1 (pu)), G=500W/m².

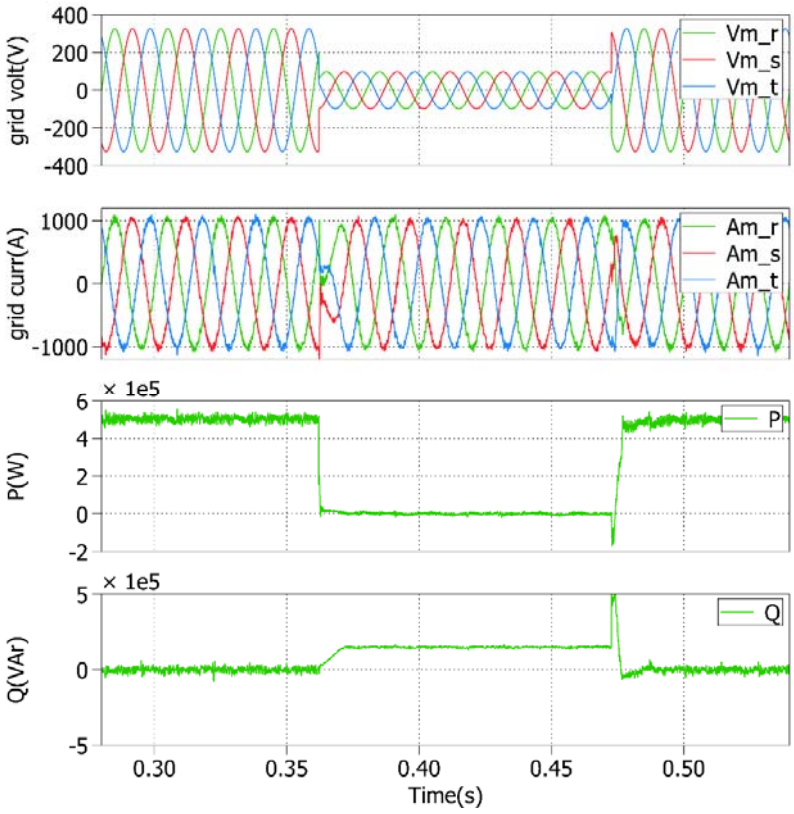

(a)

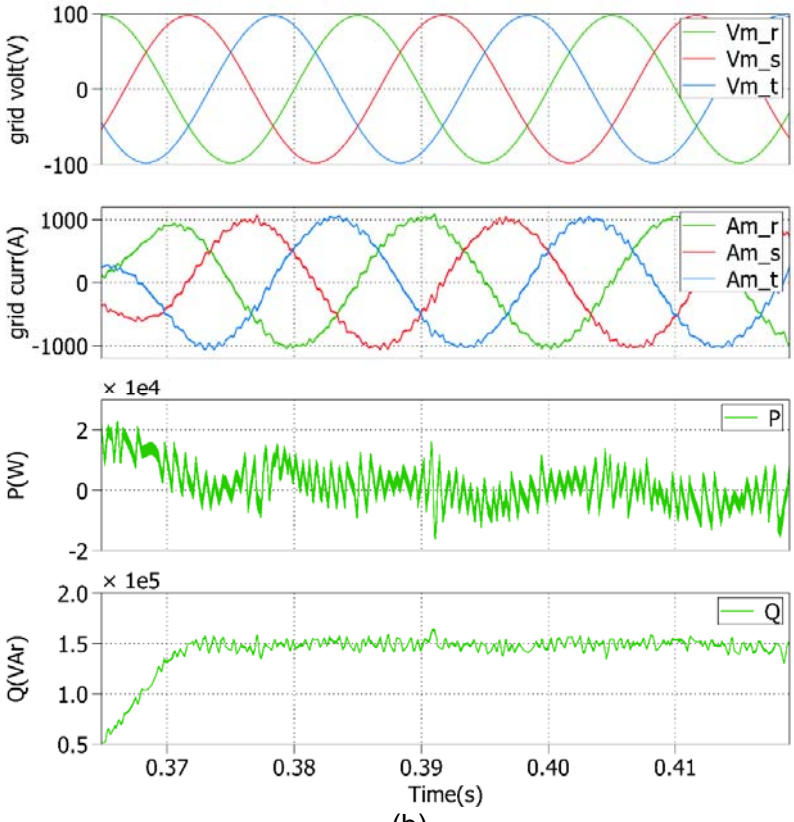

(b)

Figure 25: 3-phase deep voltage sag (0.3 (pu)), G=1000W/m².

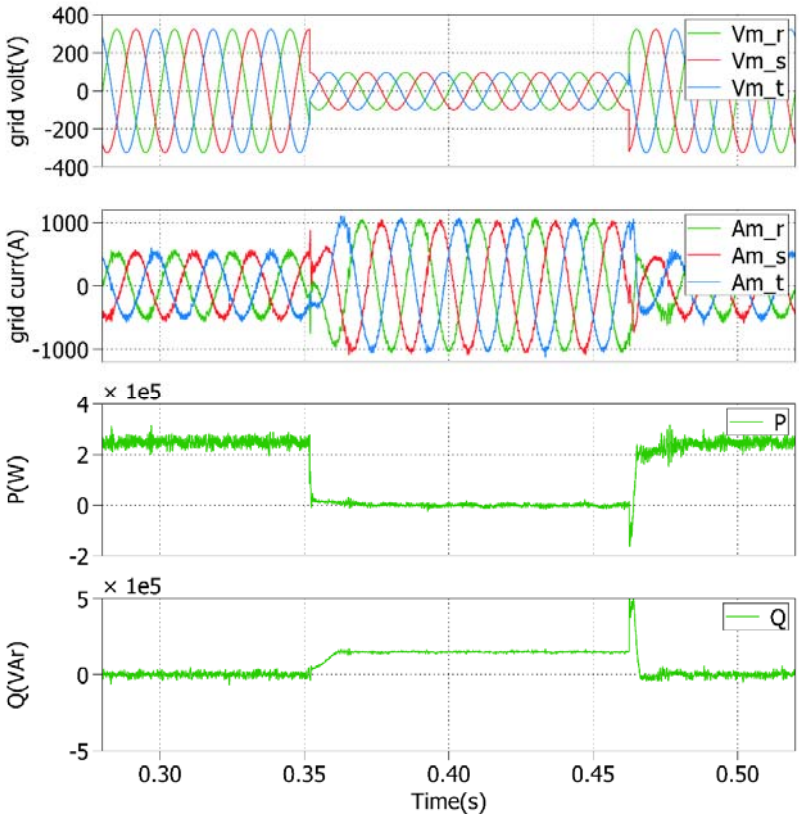

(a)

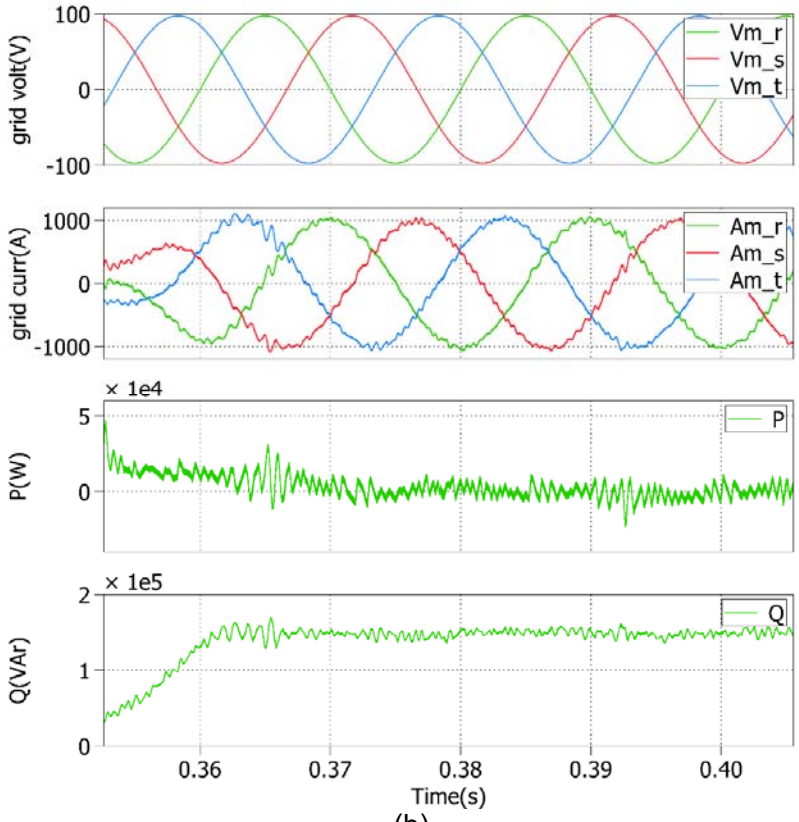

(b)

Figure 26: 3-phase deep voltage sag (0.3 (pu)), G=500W/m^2.

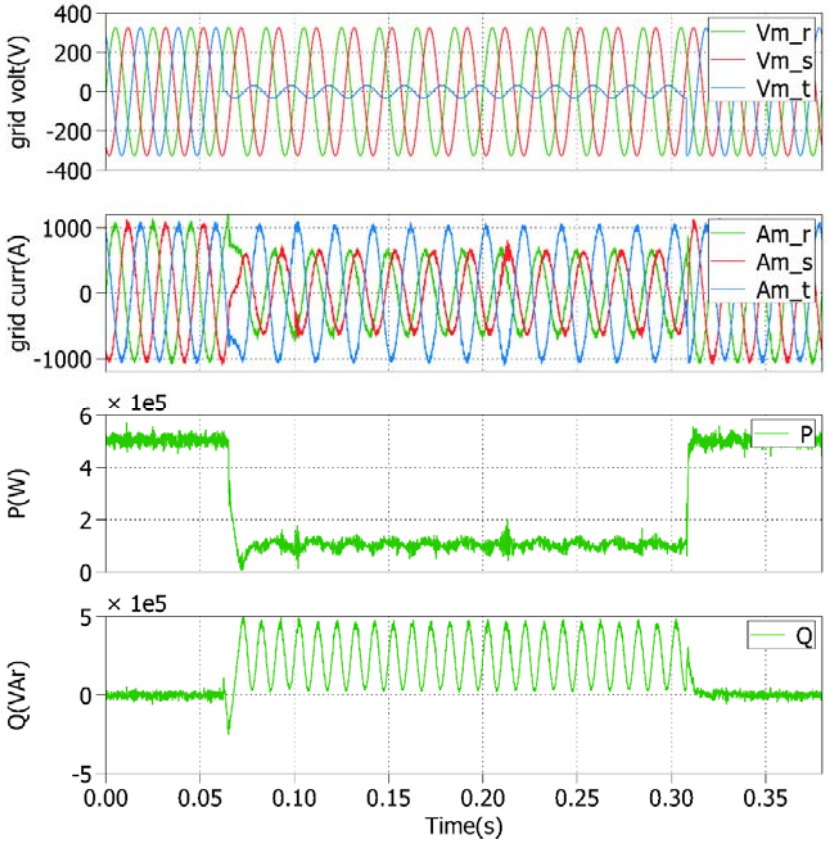

(a)

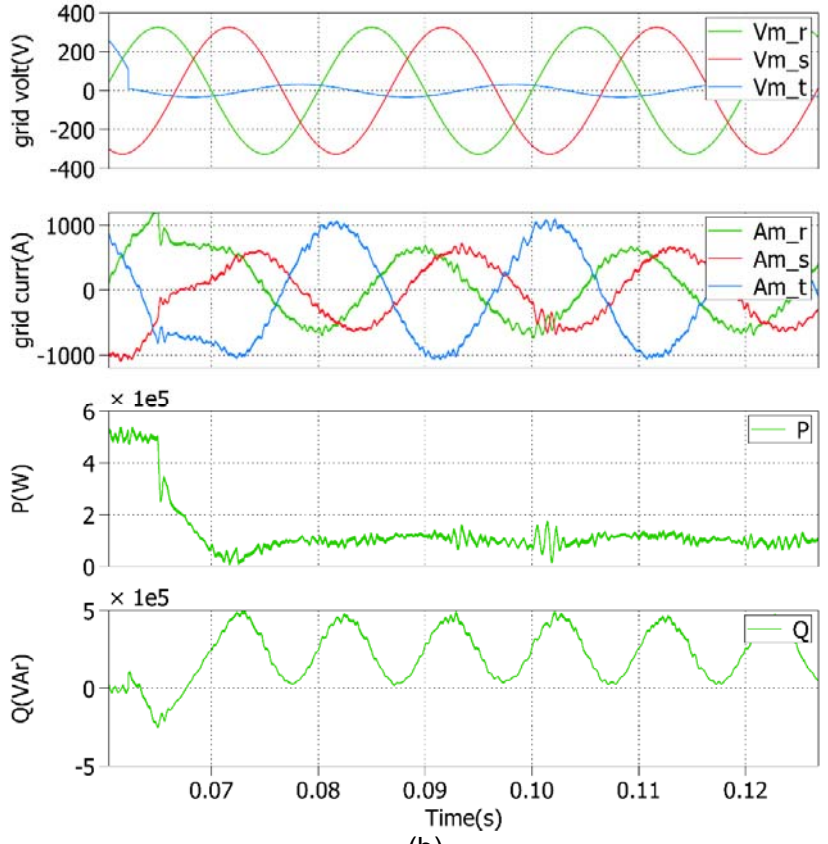

(b)

Figure 27: Deep voltage sag in phase 3 (0.1 (pu)), G=1000W/m^2.

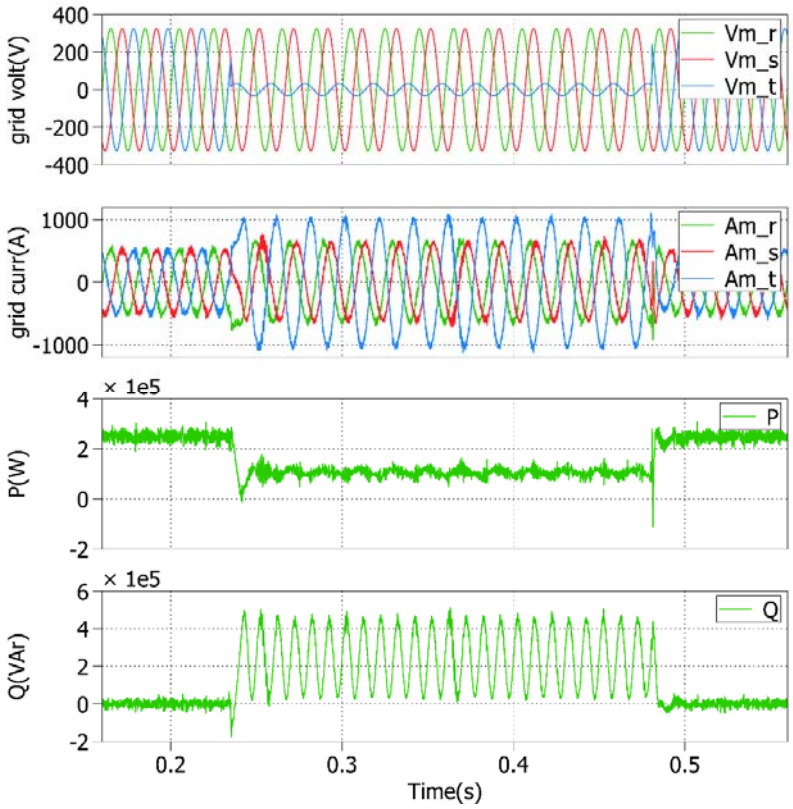

(a)

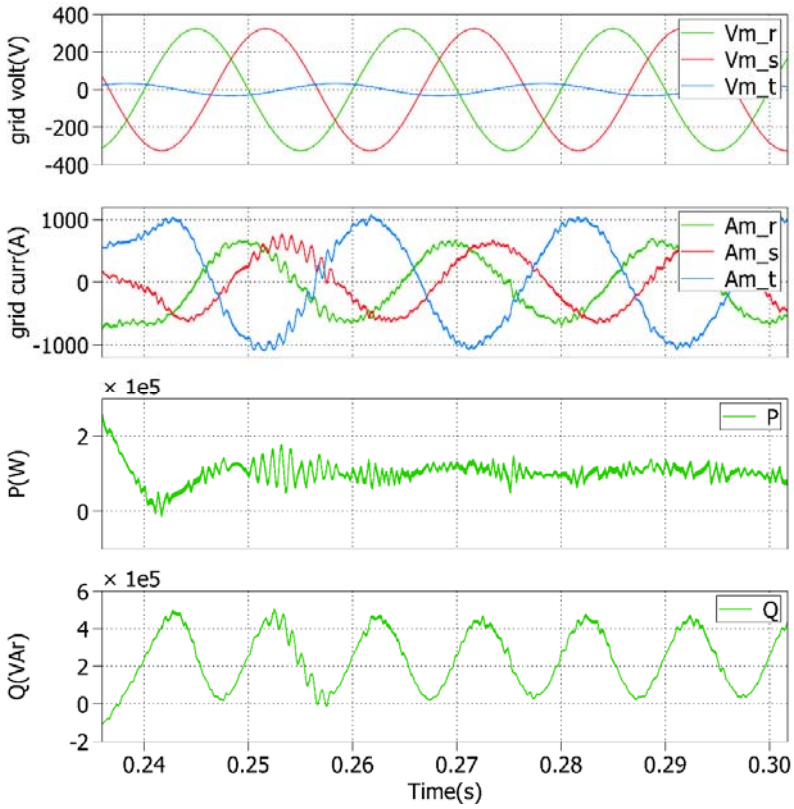

(b)

Figure 28: Deep voltage sag in phase 3 (0.1 (pu)), G=500W/m^2.

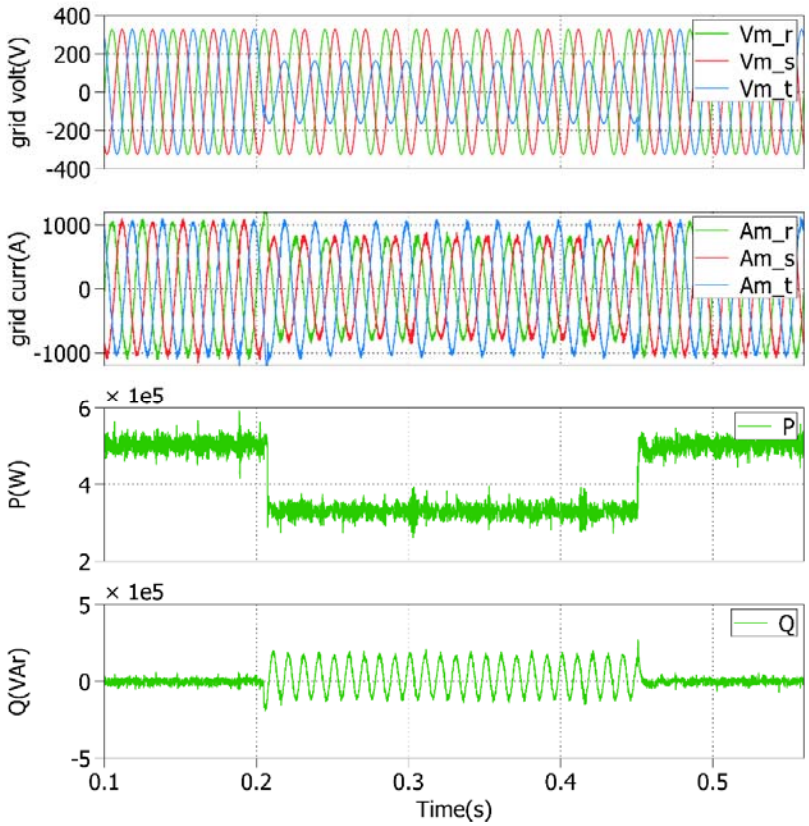

(a)

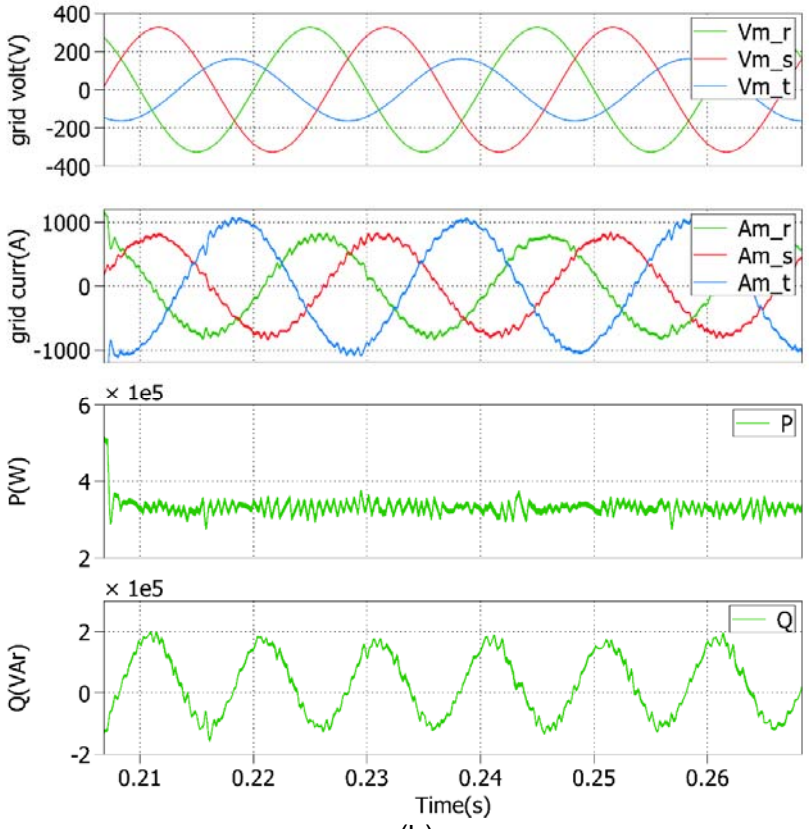

(b)

Figure 29: Moderate voltage sag in phase 3 (0.5 (pu)), G=1000W/m^2.

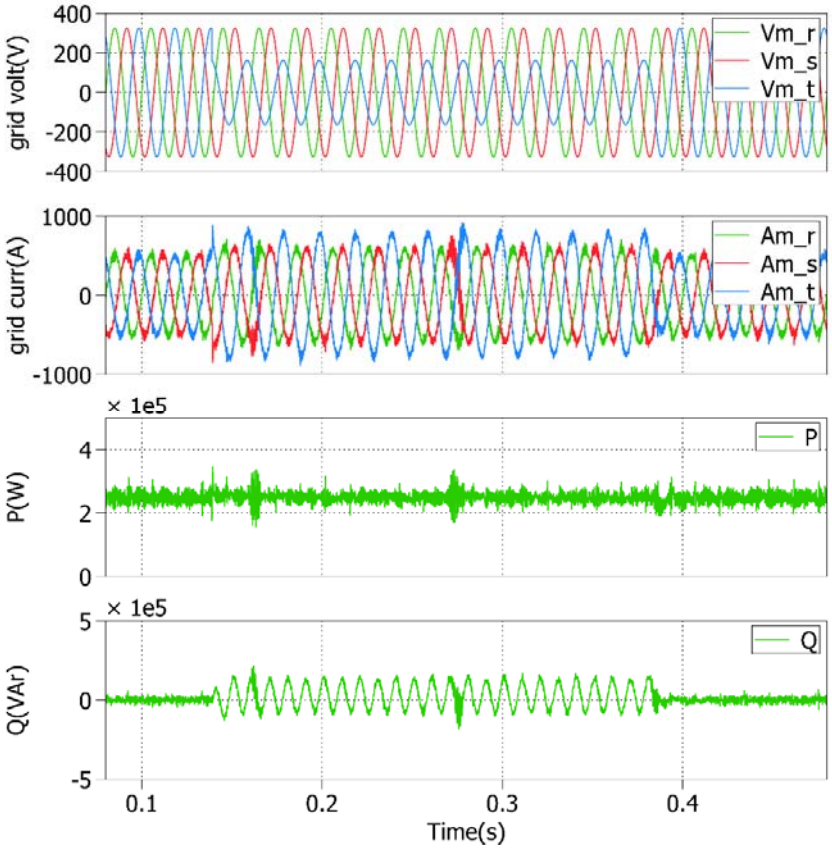

(a)

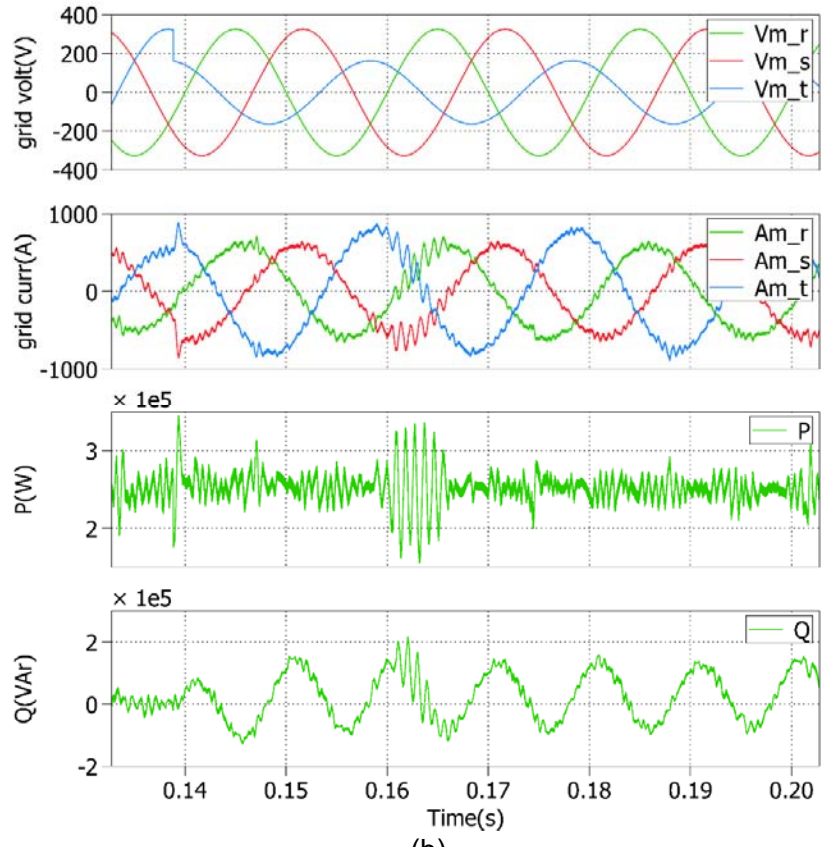

(b)

Figure 30: Moderate voltage sag in phase 3 (0.5 (pu)), G=500W/m^2.

5.2 MSOGI-FLL as the synchronization algorithm

As said before, when the nominal frequency of the 3-phase utility grid voltages varies, the conventional synchronization algorithms are not valid anymore because there will be a degradation of the power factor of the grid-connected inverter. So, a more sophisticated structure with adaptive resonant filters is mandatory. In Figure 31 (a) the block diagram of the Multiple Second-Order Generalized Integrators Frequency-Locked Loop (MSOGI-FLL) synchronization algorithm is shown [19] where multiple adaptive filters named DSOGI-QSGi (i is the harmonic to be detected) are placed in parallel, and the FLL block computes the actual fundamental frequency of the 3-phase utility grid voltages. In addition, the PNSC computes the positive- and negative- sequences of the fundamental frequency and the harmonics of the 3-phase voltages. Gain K deals with the dynamics and stability, and the FLL gain is normalized to linearize its response [3,19]. In Figure 31 (b) the block diagram of a grid-connected PV Generator using the PR controller for the 3-phase line currents with LVRT capability and adaptive frequency operation is shown. It can be seen in the latter how the measured frequency at the output of the MSOGI-FLL synchronization algorithm is feedback to the PR controllers in α-β axes in order to tune its resonant filters.

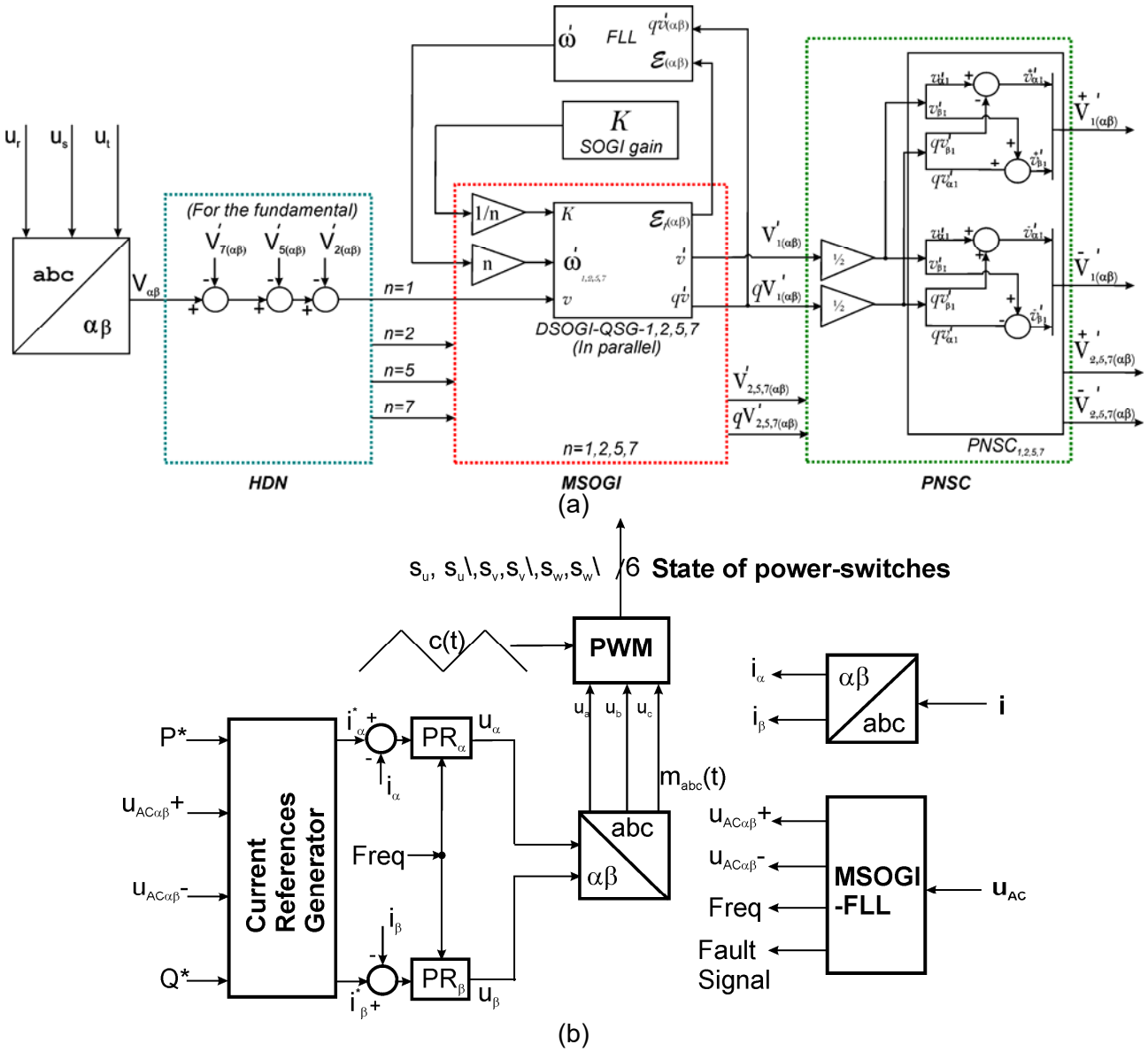

Figure 31: (a) Block diagram of the MSOGI-FLL as the synchronization algorithm.
(b) Block diagram of a grid-connected PV Generator using the PR controller for the 3-phase line currents with LVRT capability and adaptive frequency operation.

Following, some test are depicted to show the operation of the 3-phase grid-connected PV system under the frequency variation of the 3-phase utility grid voltages and with LVRT capability. Firstly, the tests for a nominal frequency of 50Hz are shown and, secondly, the same situation is depicted for a nominal frequency of 60Hz.

5.2.1 Low Voltage Ride Through with Frequency Variation. Feedback of the measured frequency to the PR controllers

5.2.1.1 Experiment 8. 50Hz

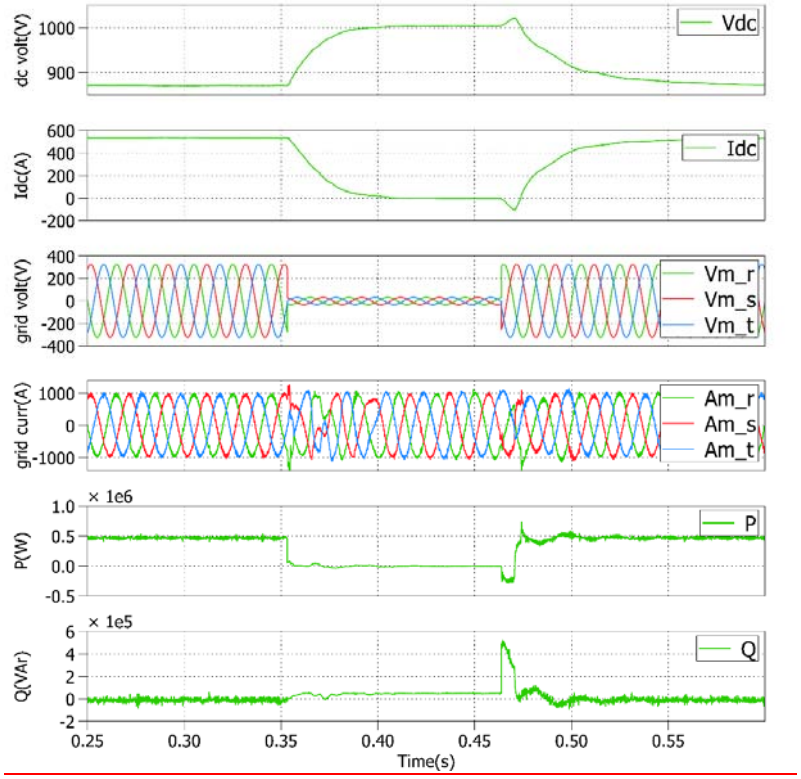

(a)

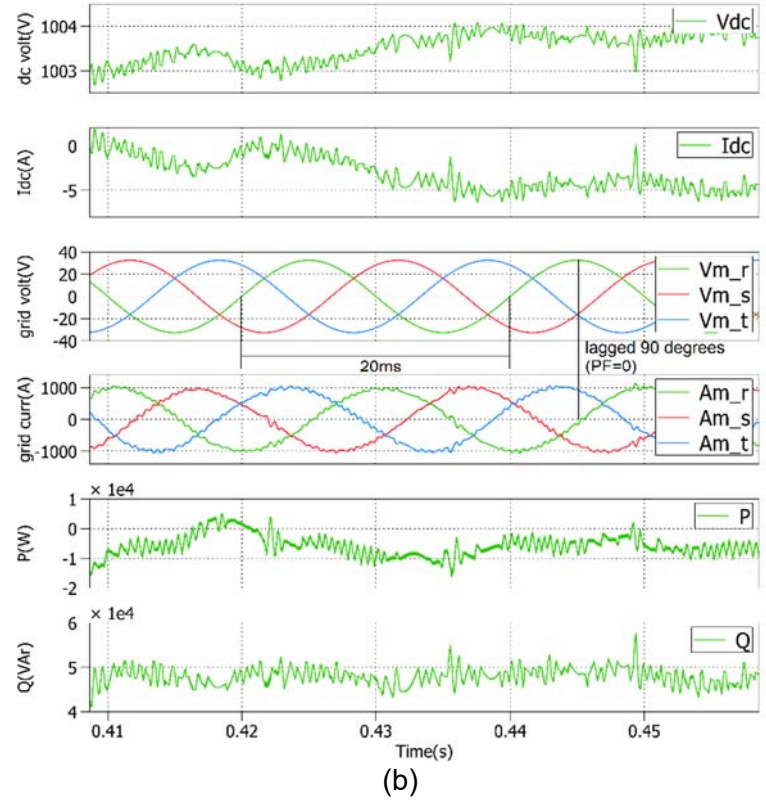

(b)

Figure 32: 3-phase deep voltage sag (0.1 (pu)), G=1000W/m².

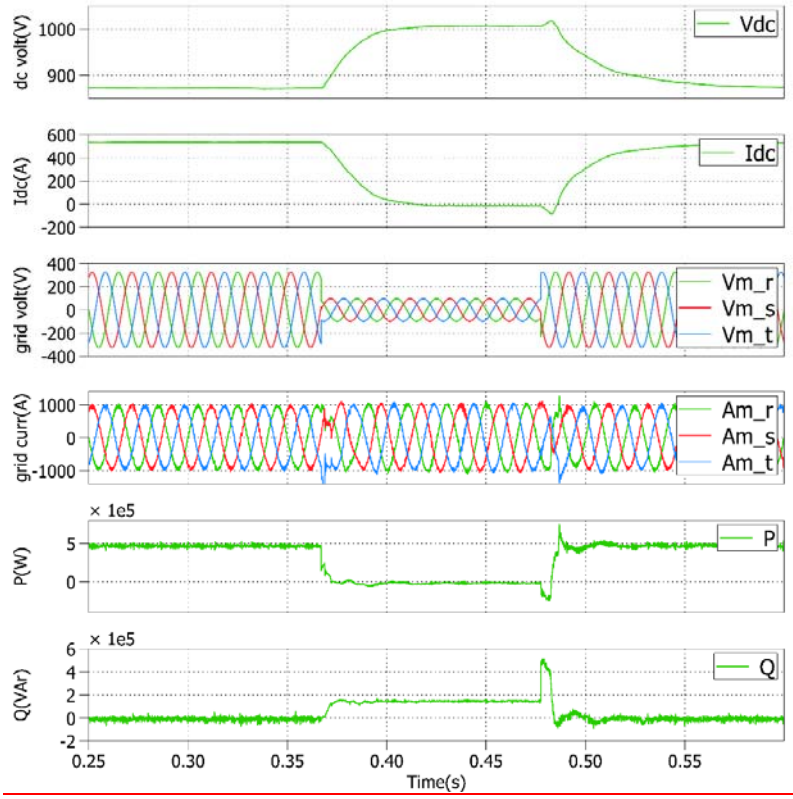

(a)

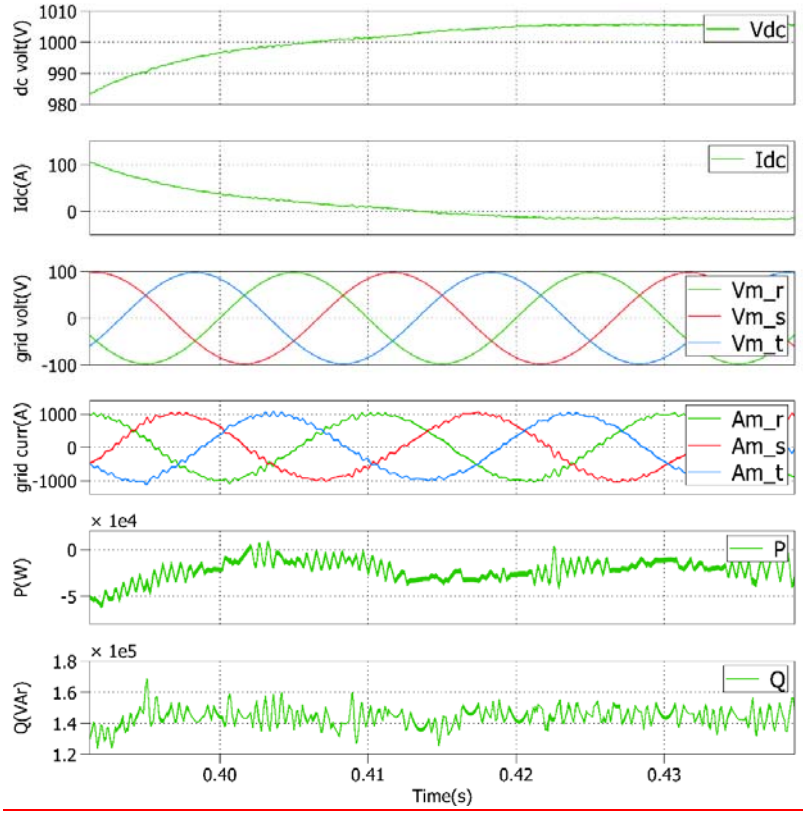

(b)

Figure 33: 3-phase deep voltage sag (0.3 (pu)), G=1000W/m².

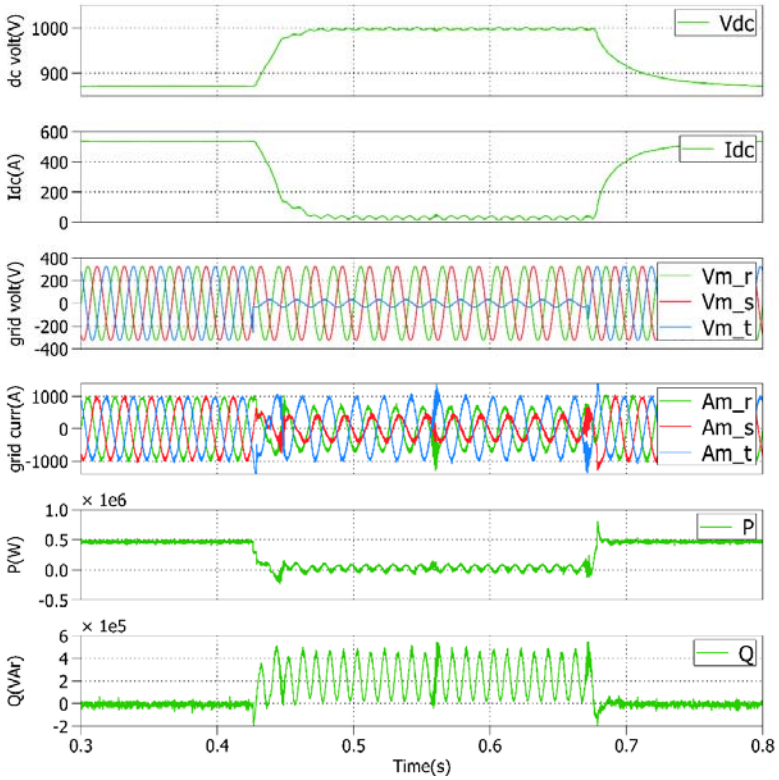

(a)

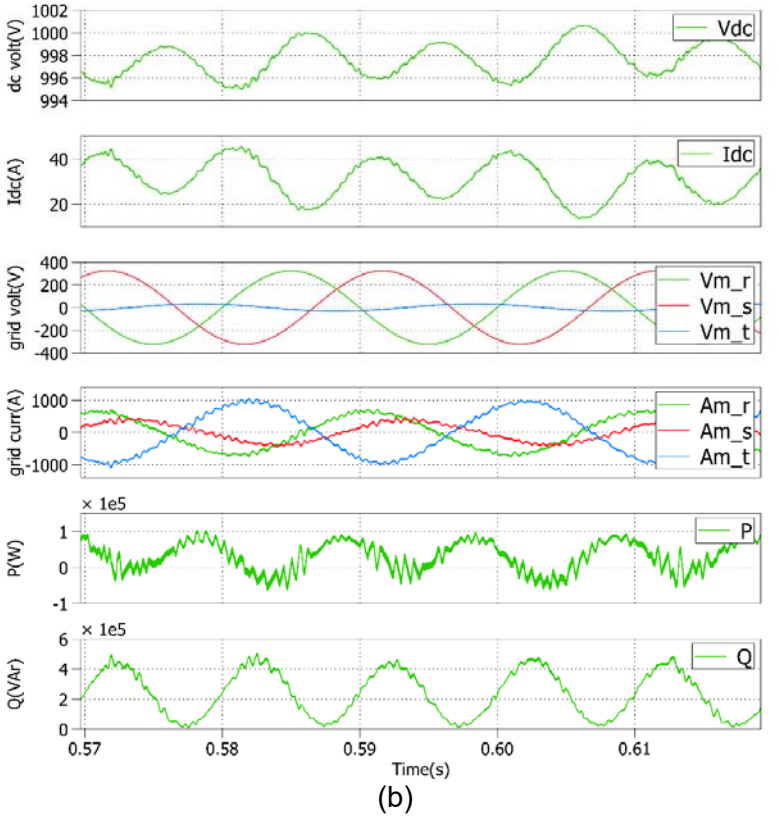

(b)

Figure 34: Deep voltage sag in phase 3 (0.1 (pu)), G=1000W/m^2.

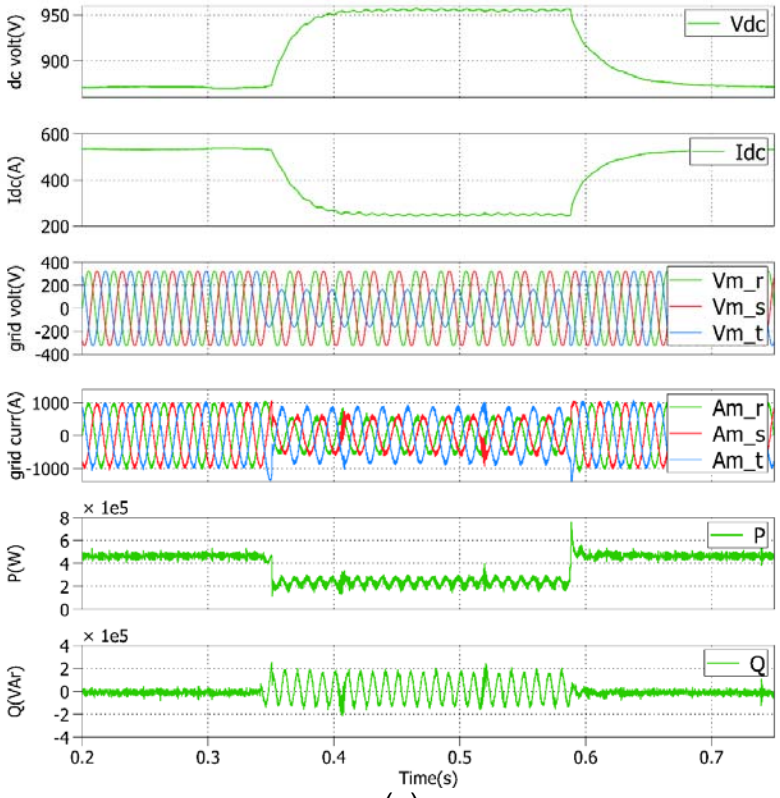

(a)

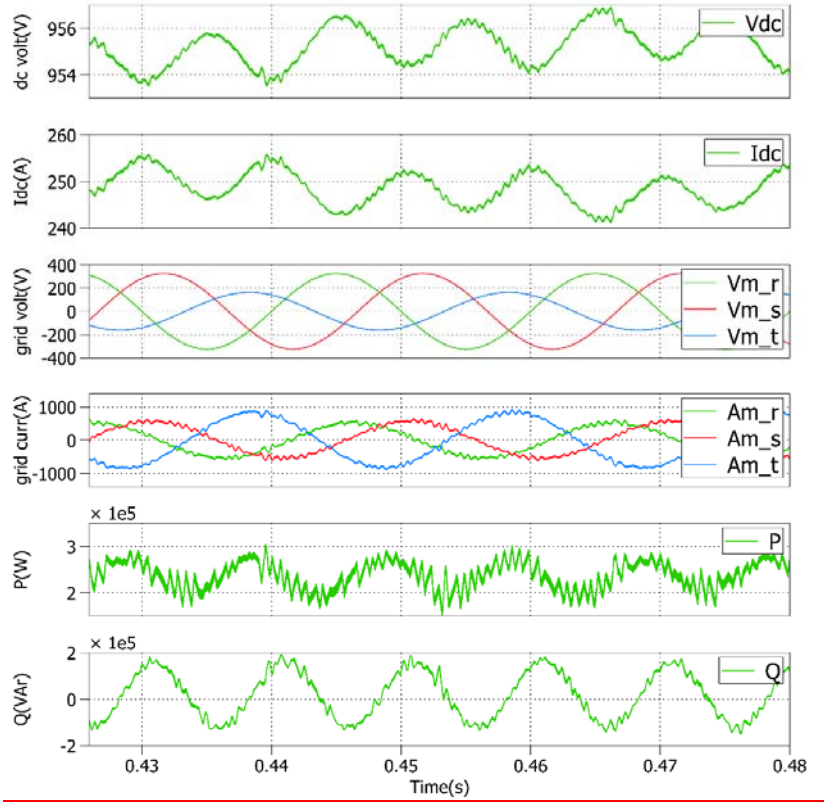

(b)

Figure 35: Moderate voltage sag in phase 3 (0.5 (pu)), G=1000W/m².

5.2.1.2 **Experiment 9.** 60Hz

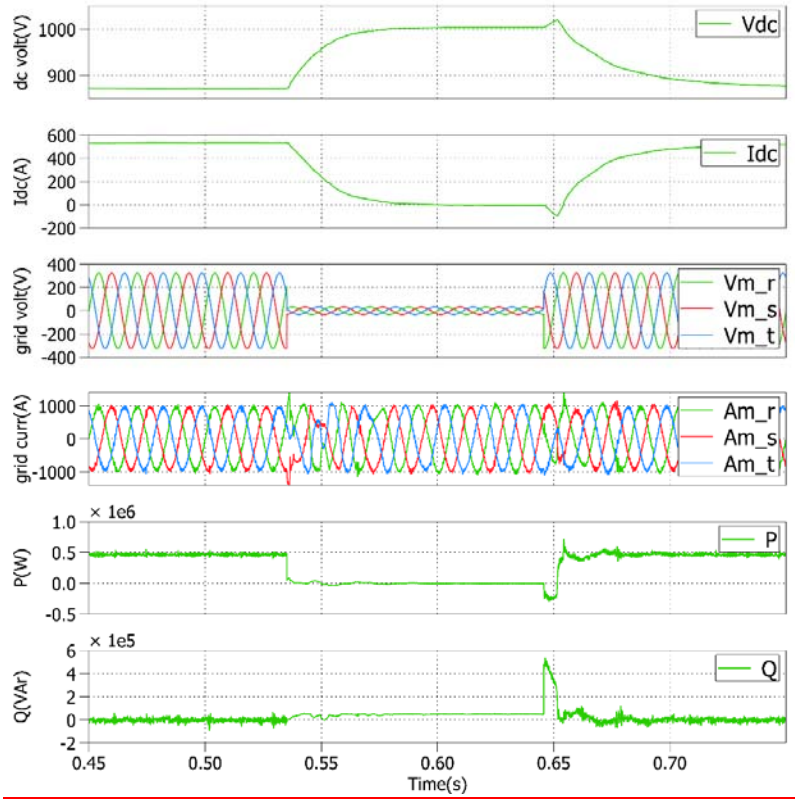

(a)

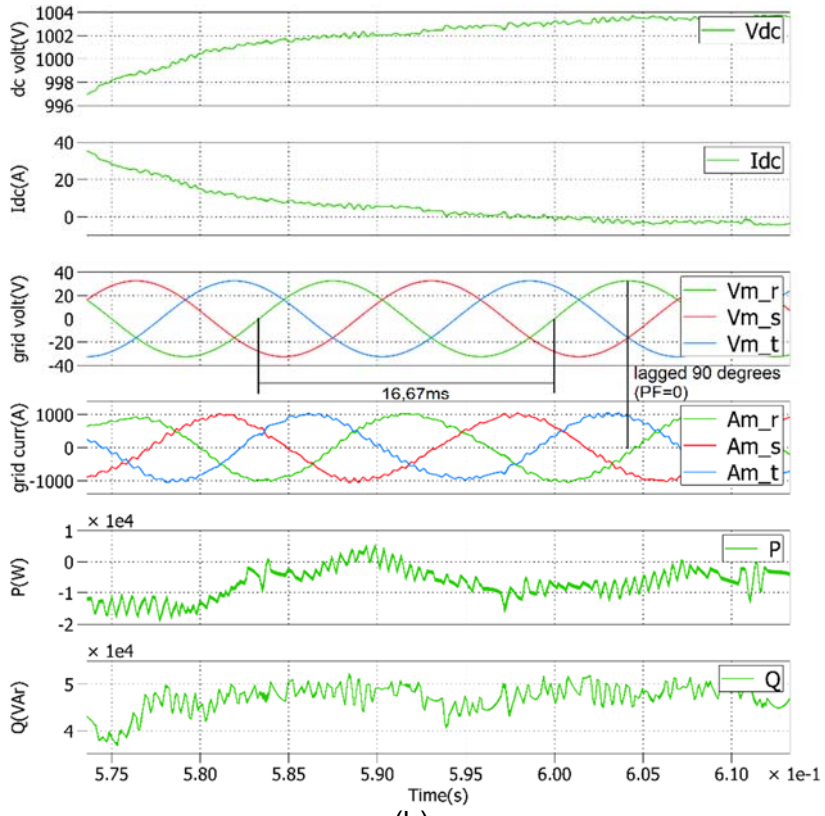

(b)

Figure 36: 3-phase deep voltage sag (0.1 (pu)), G=1000W/m².

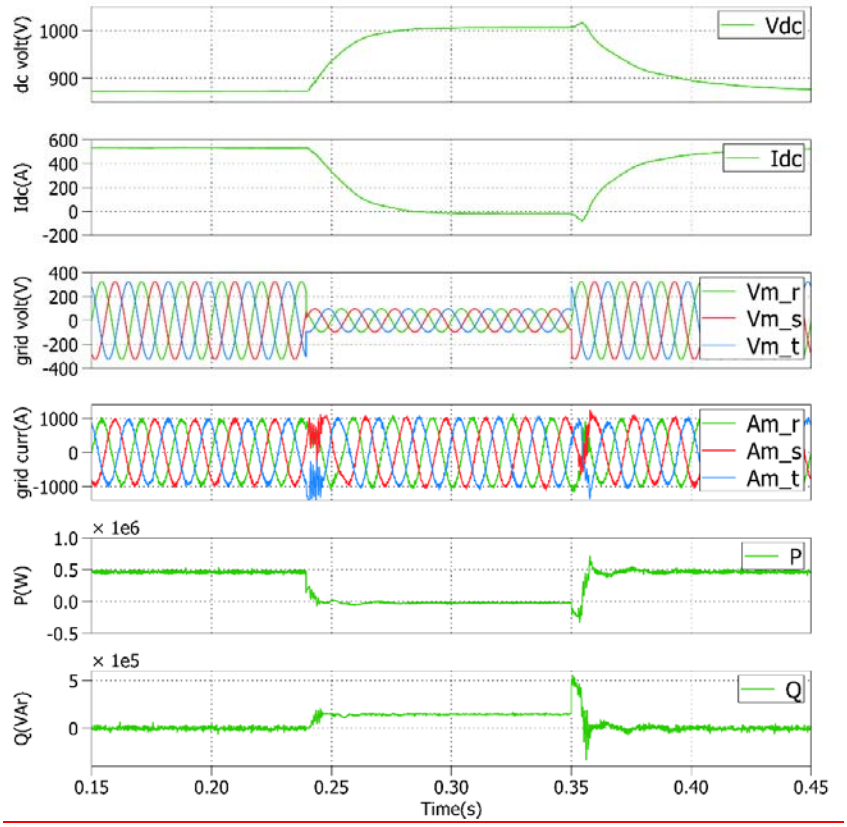

(a)

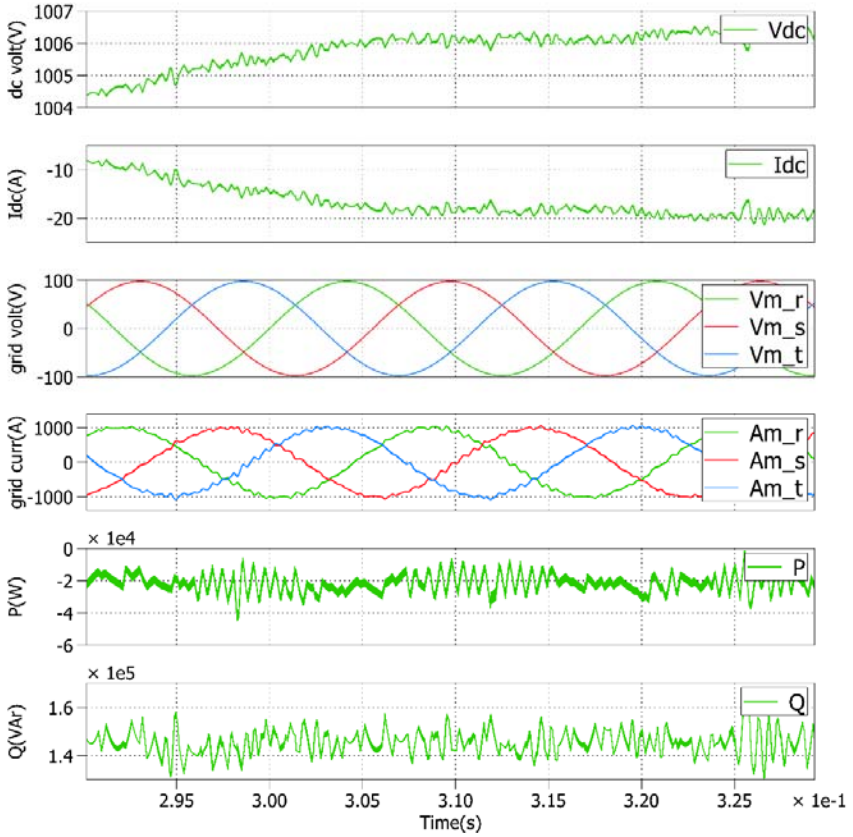

(b)

Figure 37: 3-phase deep voltage sag (0.3 (pu)), G=1000W/m^2.

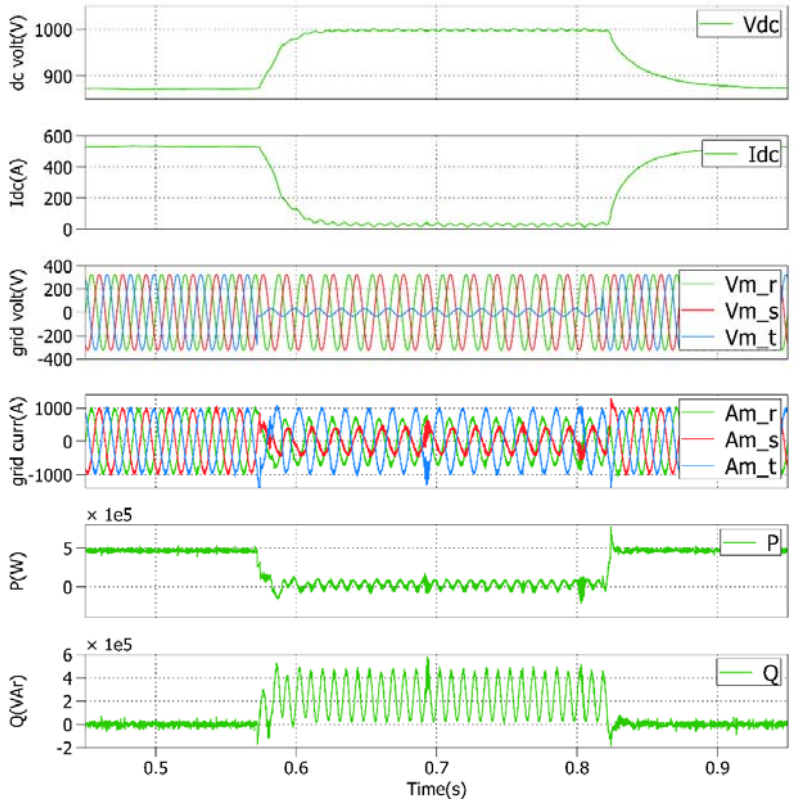

(a)

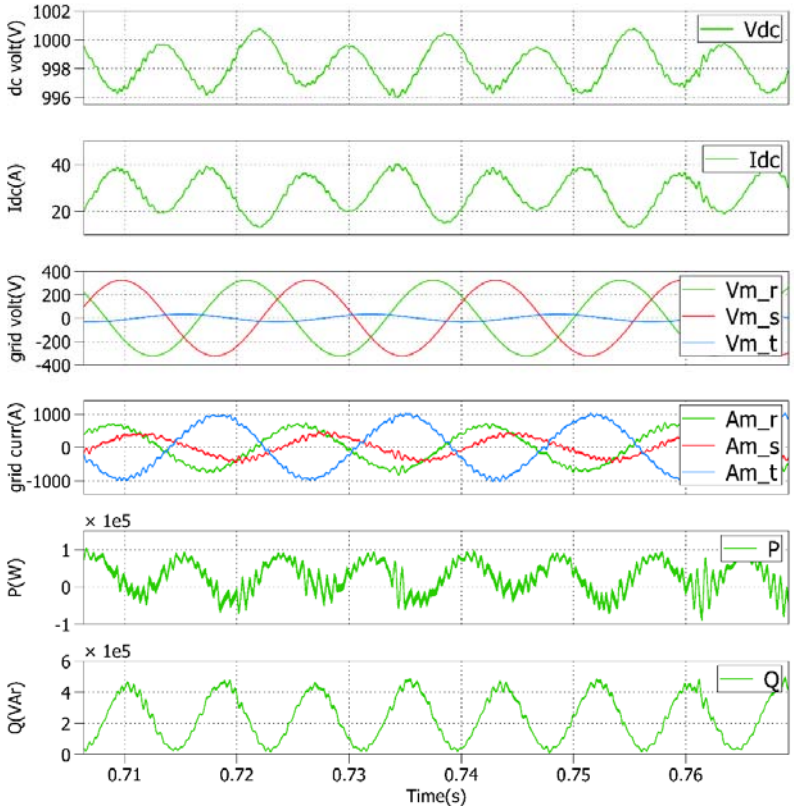

(b)

Figure 38: Deep voltage sag in phase 3(0.1 (pu)), G=1000W/m^2.

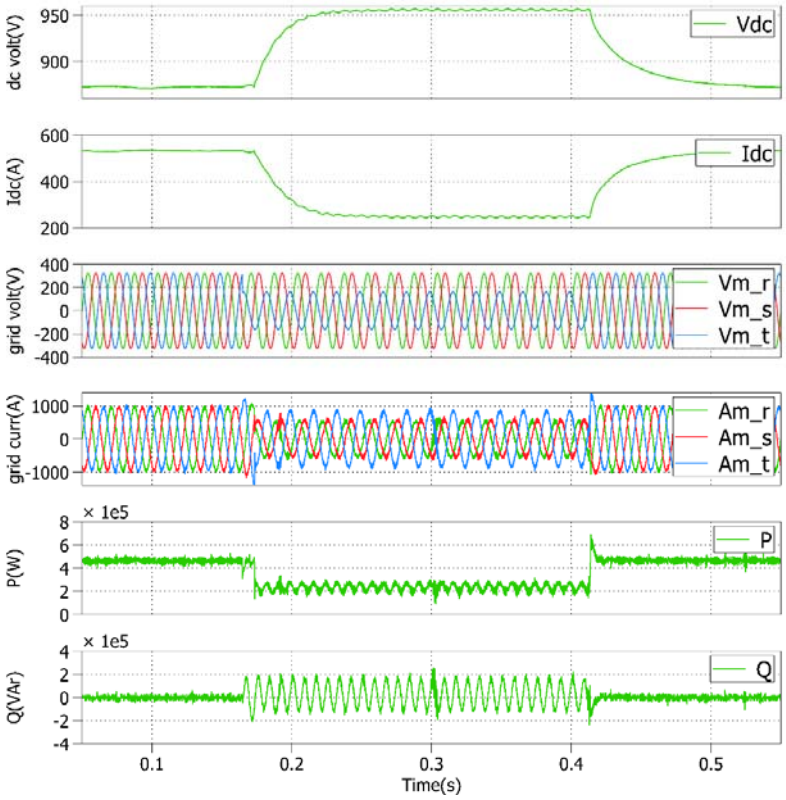

(a)

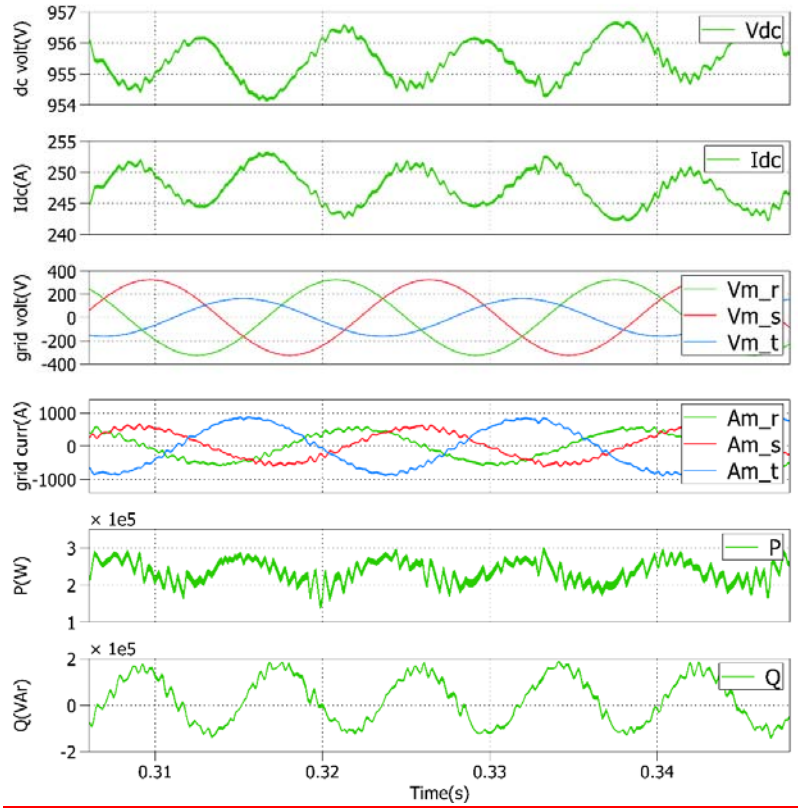

(b)

Figure 39: Moderate voltage sag in phase 3(0.5 (pu)), G=1000W/m^2.

As a conclusion of the Project it must be said that the CHIL Simulation technique was successfully implemented for the 3-phase PV grid-connected system using the PLECS RT Box 1 as the Power Subsystem and the TMS320F28379D Dual-Core Delfino Microcontroller as the Control Subsystem. Several tests were carried out in order to validate the control algorithms tested only with SIMULINK models before its implementation in this project.

Specifically, the LVRT capability was tested when several voltage sags were imposed to the 3-phase utility grid voltages. When faults occur the DC bus voltage increases to look for the new available active power in the PV system without exceeding the limits of the output inverter currents and injecting reactive power in order to improve the profile of the utility grid voltages; after the voltage sag, the DC voltage decreases until the MPP is attained, meanwhile the reactive power is set to zero for unity power factor operation.

The influence of the variation of the nominal frequency was also tested in two situations: for the conventional Positive Sequence Detector + synchronous reference frame PLL and with the enhance MSOGI-FLL algorithm. The latter guarantees the unity power factor operation due to its adaptive resonant filter when the nominal frequency of the 3-phase utility grid voltages varies.

6 Open Issues and Suggestions for Improvements

It is worth noting that during the stay at the SmartEST Lab, the user group realized that the PLECS RT Box 1 is limited in its hardware resources, mainly in the sample time of the Power Subsystem. With a sample time of around 5μs and the model of the PV Generator, a 3-phase inverter, the L filter and the 3-phase utility grid voltages with harmonics, together with the input/output signal interfaces to the Control subsystem, the use of the hardware resources was around 75%. So, the implementation of a more complex plant with several Distributed Energy Resources (DER) would be impossible if PLECS RT Box1 were used. Then, a more powerful RTDS with more hardware resources and smaller sample times, i.e. using FPGA devices, might be employed if the testing of a DG system is needed. On the contrary, no restrictions arose with the use of the TMS320F28379D Dual-Core Delfino Microcontroller as the Control Subsystem in which the control algorithms were tested.

7 Dissemination Planning

It is the intention of User Group to write at least two papers with the expected results in this project in order to possibly published them in one of the following, among others, scientific journals and/or conferences.

Journals:

- IEEE Transactions on Industry Applications
- IEEE Transactions on Industrial Informatics
- ELSEVIER Electric Power Systems Research
- ELSEVIER Energy Conversion and Management
- ELSEVIER International Journal of Electrical Power & Energy Systems

Conferences:

- IEEE International Power Electronics and Motion Control Conference (PEMC)
- IEEE International Symposium on Industrial Electronics
- Seminario Anual de Automática, Electrónica Industrial e Instrumentación (SAAEI), Spain

8 References

[1] MATLAB/SIMULINK, [Online]. Available: www.mathworks.com.

[2] N.F. Guerrero-Rodríguez, A.B. Rey-Boué. “Modelling, simulation and experimental verification for renewable agents connected to a distorted utility grid using a Real-Time Digital Simulation Platform”, *ELSEVIER Energy Conversion and Management*, vol. 84, pp. 108–121, 2014.

[3] IEC, “Electromagnetic compatibility (EMC) - Part 2-2: Environment - Compatibility levels for low-frequency conducted disturbances and signalling in public low-voltage power supply systems”, *IEC 61000-2-2*, 2002.

[4] IEEE, “IEEE Recommended practices and requirements for harmonic control in electrical power systems”, *IEEE Std. 519-1992*, 1993.

[5] IEC, “Wind turbine generator systems – Part 21: Measurement and assessment of power quality characteristics of grid connected wind turbines”, *IEC 61400-21*, 2001.

[6] E. Afshari, G. Reza, R. Rahimi, B. Farhangi, Y. Yang, F. Blaabjerg, S. Farhangi, “Control Strategy for Three-Phase Grid-Connected PV Inverters Enabling Current Limitation Under Unbalanced Faults”, *IEEE Transactions on Industrial Electronics*, vol. 64, No. 11, pp. 8908-8918, 2017.

[7] P. Rodríguez, A.V. Timbus, R. Teodorescu, M. Liserre, and F. Blaabjerg, “Flexible Active Power Control of Distributed Power Generation Systems During Grid Faults”, *IEEE Transactions on Industrial Electronics*, vol. 54, No. 5, pp. 2583-2592, 2007.

[8] R. E. Torres-Olguin, A.G. Endegnanew, and S. D'Arco, “Power-hardware-in-the-loop approach for emulating an offshore wind farm connected with a VSC-based HVDC”, *Energy Internet and Energy System Integration (EI2), 2017 IEEE Conference on*, pp. 1-6, November 2017.

[9] P. Crolla, A.J. Roscoe, A. Dysko, G.M. Burt, “Methodology for testing loss of mains detection algorithms for microgrids and distributed generation using real-time power hardware-in-the-loop based technique” *Power Electronics and ECCE Asia (ICPE & ECCE), 2011 IEEE 8th International Conference on*, pp. 833-838, 2011.

[10] dSPACE, [Online]. Available: www.dspace.com/en/pub/home.cfm

[11] OPAL-RT Technologies, [Online]. Available: www.opal-rt.com

[12] Typhoon HIL, [Online]. Available: www.typhoon-hil.com

[13] PLEXIM Electrical engineering software, [Online]. Available: www.plexim.com

[14] Texas Instruments, [Online]. Available: www.ti.com

[15] N. Jaalam, N.A. Rahim, A.H.A. Bakar, B.M. Eid, “Strategy to enhance the low-voltage ride through in photovoltaic system during multi-mode transition”, ELSEVIER Solar Energy, vol. 153, pp. 744-754, 2017.

[16] M. Karimi-Ghartemani, M.R. Iravani, “A method for synchronization of power electronic converters in polluted and variable-frequency environments”, *IEEE Transactions on Power Systems*, vol.19, pp. 1263-1270, 2004.

[17] N.F. Guerrero-Rodríguez, L.C. Herrero-de Lucas, S. de Pablo-Gómez, and A. B. Rey-Boué, “Performance study of a synchronization algorithm for a 3-phase photovoltaic grid-connected system under harmonic distortions and unbalances”. *ELSEVIER Electric Power Systems Research*, vol. 116, pp. 252-265, 2014.

[18] L.N. Arruda, S.M. Silva, B.J.C. Filho, “PLL structures for utility connected systems”. *In Proceedings of the Industry Applications Conference*, Chicago, USA, 2001.

[19] P. Rodríguez, A. Luna, I. Candela, R. Mujal, R. Teodorescu, and F. Blaabjerg, "Multiresonant Frequency-Locked Loop for Grid Synchronization of Power Converters Under Distorted Grid Conditions", *IEEE Transactions on Industrial Electronics*, vol. 58, No. 1, pp. 127-138, 2011.

9 Annex

9.1 List of Figures

9.2 List of Tables